JOC The Journal of Organic Chemistry

Article

pubs.acs.org/joc

Series of Carbazole–Pyrimidine Conjugates: Syntheses and Electronic, Photophysical, and Electrochemical Properties

Shin-ichiro Kato,[†] Yuji Yamada,[†] Hidetaka Hiyoshi,[‡] Kazuto Umezu,[‡] and Yosuke Nakamura*[,†]

[†]Division of Molecular Science, Faculty of Science and Technology, Gunma University, 1-5-1 Tenjin-cho, Kiryu, Gunma 376-8515, Japan

[‡]Ihara Chemical Industry Co., Ltd., Taito-ku, Tokyo 110-0008, Japan

Supporting Information

ABSTRACT: A series of carbazole–pyrimidine conjugates **1**–**17** were synthesized by Pd-catalyzed cross-coupling, oxidation, and nucleophilic aromatic substitution reactions. In **1**–**17**, the carbazole moieties are connected at the 4,6-positions of the pyrimidine ring either directly or via ethynylene or vinylene spacers, and various electron-donating or electron-withdrawing substituents are introduced at the 2-position of the pyrimidine ring. The effects of structural variations on the electronic, photophysical, and electrochemical properties of **1**–**17** were comprehensively investigated. Compounds **1**–**17** exhibit intramolecular charge-transfer (ICT) states, which essentially lead to moderate-to-strong fluorescence emission with large Stokes shifts depending on the solvent polarity. These compounds tend to show significant changes in optical and fluorescence properties upon addition of trifluoroacetic acid. The electron-accepting ability of these compounds can be tuned by both substituents on the pyrimidine moiety and spacers. The ethynylene spacer lowers both the HOMO and LUMO levels, while the vinylene spacer elevates the HOMO level and lowers the LUMO level. The X-ray crystal structures of **3**, **6**, **11**, and **14** are also disclosed.

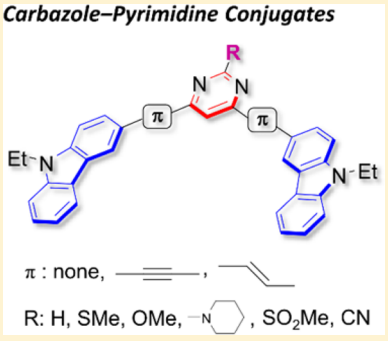

INTRODUCTION

π-Conjugated compounds bearing both electron-donating and electron-accepting moieties, so-called push–pull chromophores, are an important class of materials for optical and optoelectronic applications.[1,2] In particular, push–pull chromophores exhibiting intramolecular charge-transfer (ICT) emission have attracted tremendous research interest because of their promising applications in nonlinear optics (NLO), organic light-emitting diodes (OLEDs), and luminescence sensors.[3] The combination of electron-donating and electron-withdrawing heteroaromatics is one of the most efficient strategies to construct such push–pull fluorophores, because a judicious choice of heteroaromatics as a building block could facilitate simultaneous manipulation of the HOMO and LUMO levels and the emission color of the resulting molecules. Carbazole is one of the most important fluorescent and electron-donating heteroaromatics with rich structural diversity. Hence, oligo/polycarbazoles and related compounds are now representative benchmark materials in organic electronics.[4] Recently, the carbazole fragment has been widely used as a building block of push–pull fluorophores for various applications.[5] Particularly, after the seminal work by Adachi and co-workers,[6,7] nonplanar carbazole-based push–pull fluorophores have been extensively prepared and investigated as promising materials for OLEDs utilizing thermally activated delayed fluorescence.[8]

During the past decade, there has been strong interest in the synthesis of pyrimidine-based chromophores.[9,10] Pyrimidine has a highly π-deficient character, and its 2,4,6-positions can be easily functionalized, which makes it an appropriate electron-withdrawing heteroaromatic for the construction of push–pull architectures. Thus, a variety of donor-substituted pyrimidine derivatives, in which the electron-donating unit is linked either directly or via a π-spacer, have been recently synthesized by several research groups,[11−13] and now it is well-established that pyrimidine derivatives incorporating *N*,*N*-dialkylaniline or *N*,*N*-diarylaniline moiety at the 4,6-positions generally exhibit intense, solvatochromic fluorescence and NLO properties. The replacement of the aniline units with the electron-donating heteroaromatics would alter not only photophysical properties but also electrochemical properties reflecting the structural and electronic features of heteroaromatics. However, the exploitation of pyrimidine-based push–pull systems incorporating electron-donating heteroaromatics except for thiophene has been limited.[14,15] Additionally, the substituent effects at the 2-position of the pyrimidine ring on the properties have been hardly examined.[12a] Therefore, there is still a demand for the development of novel pyrimidine-based push–pull fluorophores.

As a part of our ongoing work toward the study on carbazole-based π-conjugated systems,[16] we envisaged that mixed π-conjugated systems consisting of carbazole and pyrimidine units would be a new class of push–pull fluorophores featuring amphoteric redox behavior. Thus, we were motivated to synthesize carbazole–pyrimidine conjugates **1**–**17** (Chart 1), in

Received: June 21, 2015
Published: August 24, 2015

DOI: 10.1021/acs.joc.5b01409
J. Org. Chem. 2015, 80, 9076−9090

Chart 1. Carbazole−Pyrimidine Conjugates 1−17

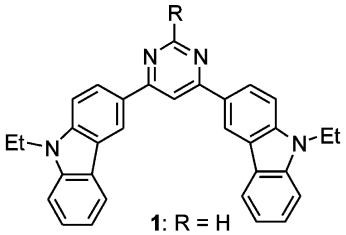

1: R = H
2: R = SMe
3: R = OMe
4: R = −N
5: R = SO_2Me
6: R = CN

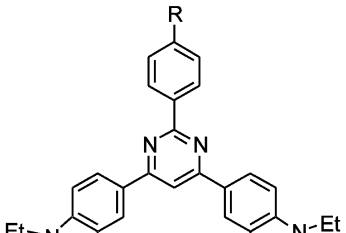

7: R = H
8: R = OMe
9: R = CN

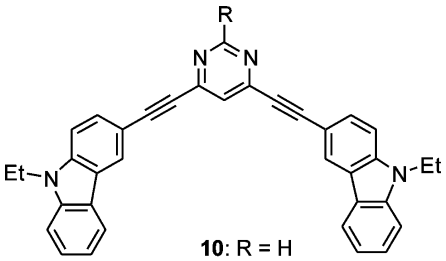

10: R = H
11: R = SMe
12: R = OMe
13: R = −N
14: R = SO_2Me
15: R = CN

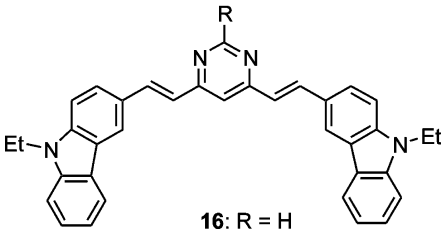

16: R = H
17: R = SMe

which the carbazole groups are connected at the 4,6-positions of the pyrimidine ring either directly or via ethynylene or vinylene spacers and various electron-donating or electron-withdrawing substituents are introduced at the 2-position of pyrimidine. Although some carbazole−pyrimidine-based conjugates have been synthesized,[15] there is no report on 4,6-bis(carbazol-3-yl)pyrimidine derivatives so far. The comprehensive study on physicochemical properties of a large series of **1**−**17** should permit researchers to establish the general and useful structure−property relationships of carbazole−pyrimidine conjugates and potentially lead to customization of photophysical and electrochemical properties for specialized materials design. We describe herein the synthesis, the structural features, and the electronic, photophysical, and electrochemical properties of **1**−**17** on the basis of X-ray crystallographic analyses, UV−vis and fluorescence spectral measurements, fluorescence lifetime measurements, differential pulse voltammetry, and quantum chemical calculations. The fluorescence solvatochromism and acid-responsive optical properties are also evaluated.

RESULTS AND DISCUSSION

Synthesis. The procedures used to synthesize carbazole−pyrimidine conjugates **1**−**17** are summarized in Schemes 1−6.

Scheme 1. Synthesis of 1 and 2

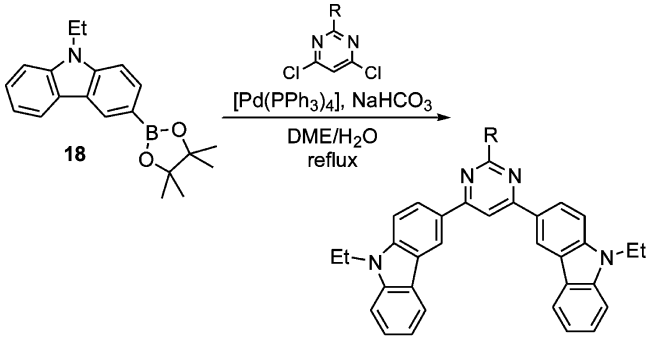

1: R = H (88%)
2: R = SMe (95%)

Scheme 2. Synthesis of 3−6

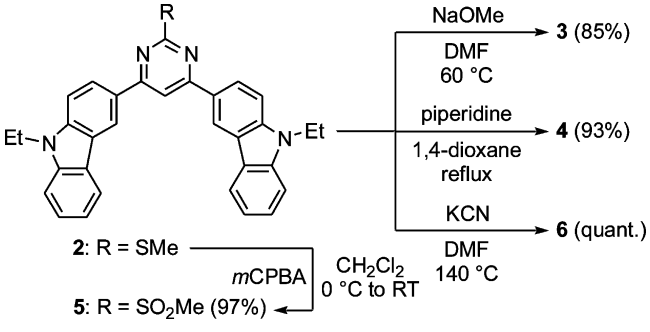

With the use of commercially available 4,6-dichloropyrimidine or 4,6-dichloro-2-(methylsulfanyl)pyrimidine as a starting material, **1**−**17** were synthesized within four steps via the Pd-catalyzed cross-coupling, oxidation, and nucleophilic aromatic substitution (S_NAr) reactions. As shown in Scheme 1, compounds **1** and **2** were prepared by the Suzuki−Miyaura coupling[17] with boronic acid pinacol ester **18** and the corresponding dichloropyrimidines in 88% and 95% yields, respectively.

As shown in Scheme 2, compound **2** was oxidized to methylsulfonylpyrimidine **5** in 97% yield using *m*CPBA as an oxidant. Compound **5** was subjected to the S_NAr reactions with

DOI: 10.1021/acs.joc.5b01409
J. Org. Chem. 2015, 80, 9076−9090

Scheme 3. Synthesis of 7−9

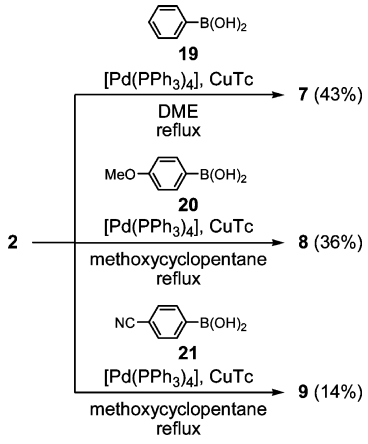

Scheme 4. Synthesis of 10 and 11

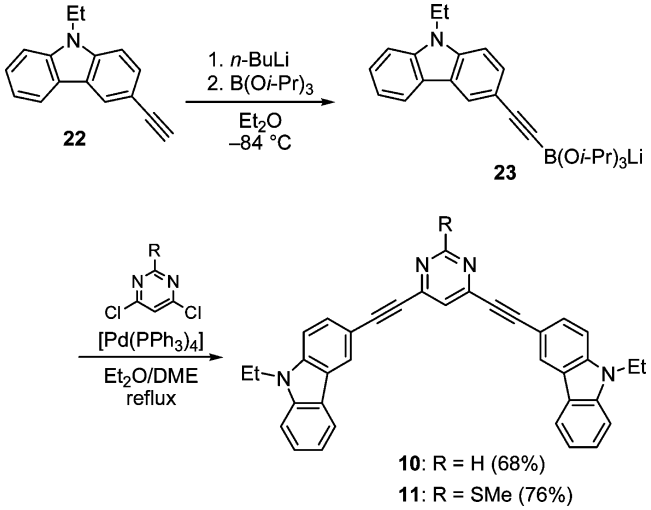

Scheme 5. Synthesis of 12−15

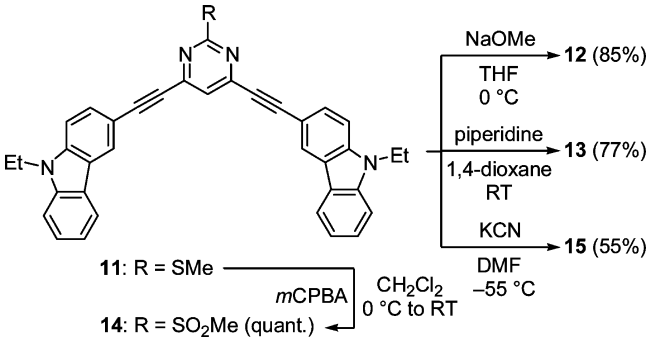

NaOMe, piperidine, and KCN to afford **3**, **4**, and **6**, respectively, in high yields.[18]

Compounds **7**−**9** were prepared by the Liebeskind−Srogl coupling reaction of **2** with the corresponding phenylboronic acids **19**−**21** (Scheme 3), where $[Pd(PPh_3)_4]$ catalyst and copper(I) thiophene-2-carboxylate (CuTc) cocatalyst were used.[19] The reactions of **2** with **19**−**21** were so slow that **2** was not entirely consumed even though **2** was allowed to react with an excess amount of **19**−**21** for more than 18 h.[20]

The synthesis of **10** and **11** was outlined in Scheme 4. The Sonogashira reaction of 3-ethynyl-9-ethyl-9*H*-carbazole (**22**) and 4,6-dichloro-2-(methylsulfanyl)pyrimidine with $[PdCl_2(PPh_3)_2]$ catalyst and CuI cocatalyst produced no desired **11**, and homocoupling product of **22** was exclusively obtained (Scheme S1 in the Supporting Information). Therefore, we applied the Suzuki−Miyaura coupling for sp−sp^2 carbon bond formation by using an organoboron acetylide. The "ate-complex" **23** was generated *in situ* by lithiation of **22** with *n*-BuLi and subsequent reaction with triisopropoxyborane,[21] and then subjected to the Pd-catalyzed cross-coupling reaction with 4,6-dichloro-2-(methylsulfanyl)pyrimidine to afford **11** in 76% yield. By the similar cross-coupling procedure, **10** was synthesized in 68% yield.

Scheme 6. Synthesis of 16 and 17

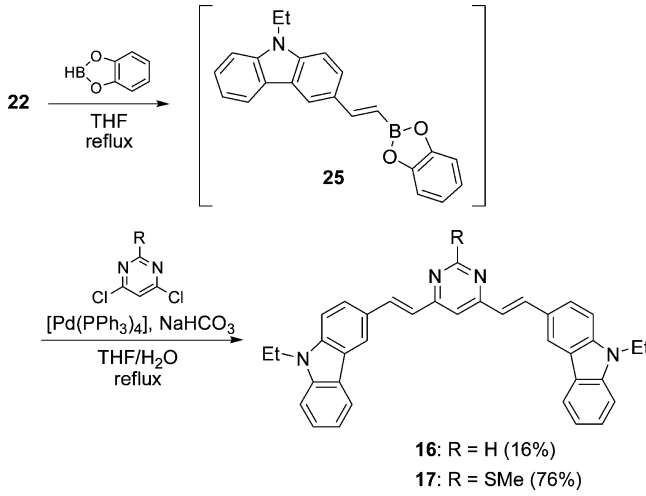

The *m*CPBA oxidation of **11** gave **14** quantitatively, and the following S_NAr reactions of **14** with the corresponding nucleophiles afforded **12**, **13**, and **15** in moderate-to-high yields (Scheme 5). We found that the S_NAr reactions of **14** proceeded at a lower temperature than those of **5**. The higher electrophilicity of **14** than **5** should stem from electron-withdrawing ability of the ethynylene segments in **14**.

The Heck reaction of 3-ethenyl-9-ethyl-9*H*-carbazole (**24**) with 4,6-dichloro-2-(methylsulfanyl)pyrimidine by using a catalyst/base system of $[Pd(OAc)_2]$ and $(o\text{-tolyl})_3P/Et_3N$ afforded no desired **17** and resulted in a quantitative recovery of starting materials (Scheme S2 in the Supporting Information). As shown in Scheme 6, we applied *in situ* preparation of **25** by hydroboration of **22** using catecholborane and the subsequent Suzuki−Miyaura coupling of **25** with 4,6-dichloro-2-(methylsulfanyl)pyrimidine in a catalyst/base system of $[Pd(PPh_3)_4]/Na_2CO_3$ to afford *E*,*E*-**17** in 76% yield.[27] In a similar manner, *E*,*E*-**16** was obtained in 16% yield.[23] The low yield of *E*,*E*-**16** is apparently due to the repeated column chromatography to remove *E*,*Z*- and/or *Z*,*Z*-stereoisomers. The *m*CPBA oxidation of *E*,*E*-**17** gave not only the *E*,*E*-methylsulfonylpyrimidine derivative as a major product but the configurational isomers as minor products, and isolation of the former was unsuccessful even after numerous attempts (Scheme S3). Therefore, we abandoned further transformation of *E*,*E*-**17**.

All the compounds **1**−**17** were fully characterized by various spectroscopic methods. The stereochemistry of the vinylene moieties in **16** and **17** was established on the basis of the coupling constant for vinylic protons in the ^{1}H NMR spectra ($J \approx 16$ Hz). We found very slow isomerization of **16** in

DOI: 10.1021/acs.joc.5b01409
J. Org. Chem. 2015, 80, 9076−9090

chloroform or dichloromethane upon irradiation of room light:[24] the solution samples of **16** and **17** for spectroscopic measurements were prepared under the careful protection of room light.

Structural Properties. The single crystals of **3**, **6**, **11**, and **14** suitable for X-ray crystallographic analyses were successfully obtained (Figure 1). The solid-state structures of **3**, **6**, **11**, and

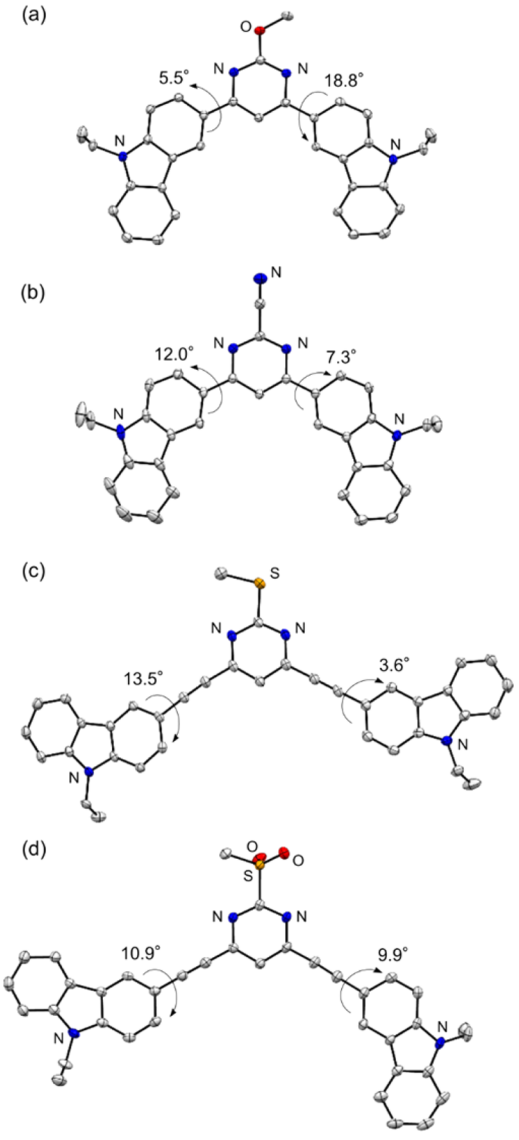

Figure 1. X-ray crystal structures of (a) **3**, (b) **6**, (c) **11**, and (d) **14**. Displacement ellipsoids are shown at the 50% probability level. Hydrogen atoms and solvent molecules are omitted for clarity.

14 are quasiplanar with torsion angles between the pyrimidine and carbazole moieties of 3.6°−18.8°, suggesting the effective π-conjugation between the two heteroaromatic components. The molecules of **3** and **6** accept the two-*cisoid* conformation between the pyrimidine ring and the carbazole π-system. The molecules of **11** adopt the two-*transoid* conformation, while those of **14** adopt the *cisoid* and *transoid* conformations. In all the crystal structures, no noticeable bond-length alternation is observed.[25]

As shown in Figure 2, the 1D column structures through effective $\pi-\pi$ stacking interactions are formed in the crystal structures of **3**, **6**, and **14**.[26] The molecules of **3** are packed in a

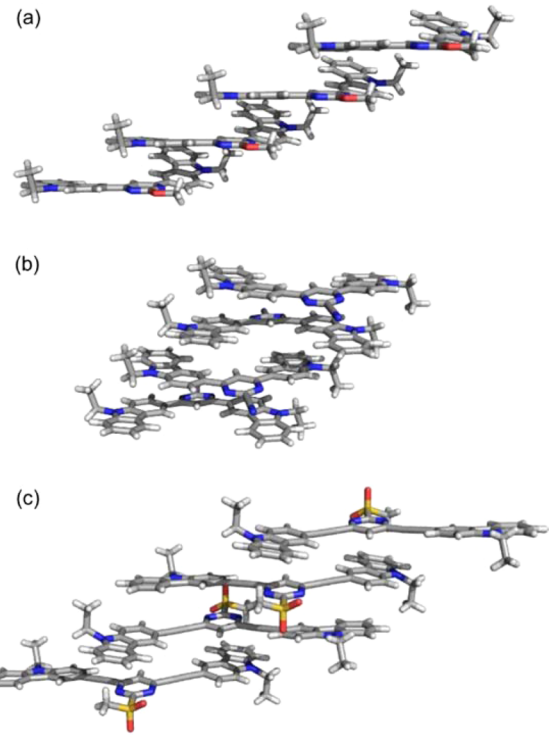

Figure 2. Molecular packing of crystals of (a) **3**, (b) **6**, and (c) **14**. Solvent molecules are omitted for clarity. The packing structures including solvent molecules are shown in Figure S1 of the Supporting Information.

head-to-head manner (Figure 2a), while the molecules of **6** and **14** are packed in a head-to-tail manner (Figure 2b,c). Interestingly, in any of these cases, the electron-donating carbazole moieties overlap with the electron-withdrawing pyrimidine moieties with distances 3.37−3.47 Å, implying that the intermolecular D−A interactions between the carbazole and pyrimidine moieties are a major driving force to form the observed 1D column structures. In the crystal packing for **11**, almost no effective $\pi-\pi$ stacking interaction is observable (Figure S1 in the Supporting Information)

Electronic Properties. The electronic absorption spectra of **1**−**17** in THF are shown in Figure 3, and their longest wavelength absorption maxima (λ_{max}^{abs}) are summarized in Table 1. In the series of **1**−**6**, the compounds except for **4** exhibit similar absorption bands in the region 320−420 nm with molar extinction coefficients ε of 32 000−39 800 mol^{-1} L cm^{-1} (Figure 3a). Compound **4** displays the broadened absorption band in the longer wavelength region and the decreased ε value (22 300 mol^{-1} L cm^{-1}) at the longest λ_{max}^{abs} (367 nm) when compared to **1**−**3**, **5**, and **6**. This implies that the piperidyl substituent in **4** contributes to the large electronic perturbation of the pyrimidine moiety. The longest λ_{max}^{abs} values of **2**−**6** are red-shifted relative to that of **1** (360 nm) by 6−21 nm, and the introduction of electron-withdrawing SO_2Me and CN groups brings about more pronounced red-shifts than electron-donating SMe and OMe groups. The longest λ_{max}^{abs} values of **7**−**9** are almost the same as those of the corresponding **1**, **3**, and **6**, indicating that the benzene ring at the 2-position has almost no effect on extension of π-conjugation (Figure 3b).

The longest λ_{max}^{abs} value of **10** is red-shifted relative to that of **1** by 22 nm (Figure 3c). The decrease in the optical

DOI: 10.1021/acs.joc.5b01409
J. Org. Chem. 2015, 80, 9076−9090

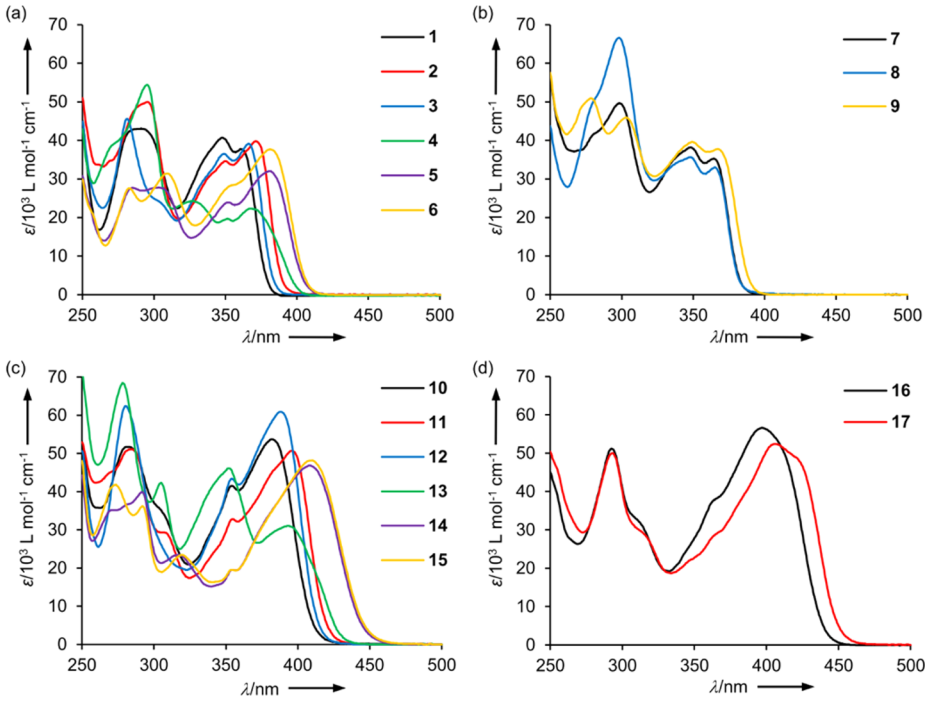

Figure 3. Electronic absorption spectra of (a) **1**–**6**, (b) **7**–**9**, (c) **10**–**15**, and (d) **16** and **17** in THF at RT.

Table 1. Photophysical Properties of 1–17 in THF[a]

	λ_{max}^{abs}/nm	λ_{max}^{fl}/nm	$\Delta\nu_{fl-abs}$/cm^{-1}	Φ_f[b]	τ_f[c]/ns	k_r[d]/10^7 s^{-1}	k_{nr}[e]/10^7 s^{-1}
1	360	395	2460	0.44	1.86	24	30
2	371	394	1570	0.23	1.03	22	74
3	366	388	1550	0.48	1.62	30	32
4	367	408	2740	0.15	1.35	11	63
5	381	426	2770	0.61	2.31	26	17
6	381	427	2830	0.63	2.57	24	14
7	364	391	1900	0.38	1.77	21	35
8	365	385	1420	0.45	1.63	27	34
9	367	408	2740	0.08	5.14	1.5	18
10	382	451	4010	0.74	2.32	32	11
11	396	449	2980	0.61	1.82	34	21
12	388	445	3300	0.63	2.04	31	18
13	393	445	2970	0.21	2.90	7.2	27
14	408	496	4350	0.74	4.22	18	6.1
15	410	495	4190	0.66	4.26	15	7.9
16	397	463	3590	0.25	*f*	*f*	*f*
17	406	464	3080	0.25	*f*	*f*	*f*

[a]The complete data of **1**–**17** in various solvents are summarized in Tables S1–S3 in the Supporting Information. [b]Absolute fluorescence quantum yields determined by an integrating sphere system. [c]Fluorescence lifetime. [d]Radiative decay constant. [e]Nonradiative decay constant. [f]The emission decay profiles were not fitted by single exponential kinetics.

HOMO–LUMO gap in **10** as compared to **1** is attributed to the effective extension of π-conjugation.[27] The substituent effects on the longest λ_{max}^{abs} values in the series of **10**–**15** are almost the same as those in **1**–**6**. Thus, when compared to **10**, the longest λ_{max}^{abs} values of **11**–**15** are exclusively red-shifted, and the extent of red-shifts in **14** and **15** having electron-withdrawing substituents are noticeable (382 nm (**10**), 408 nm (**14**), 410 nm (**15**)). The ε values in the longer wavelength region of **10**–**15** are larger than those of the corresponding **1**–**6** due to the hyperchromic effect of the alkynyl moieties. As shown in Figure 3d, the longest λ_{max}^{abs} values of **16** (397 nm) and **17** (406 nm) are further red-shifted compared to **10** and **11**, respectively, demonstrating that the vinylene spacer decreases the optical HOMO–LUMO gap more efficiently than the ethynylene spacer in carbazole–pyrimidine conjugates.[28] The ε values of **16** and **17** around the longest λ_{max}^{abs} are similar to those of **10** and **11**, respectively.

Fluorescence Properties. All the compounds in this study are fluorescent. Figure 4 shows the fluorescence spectra of **1**–**17** in THF, and their relevant photophysical data are summarized in Table 1. The color of the fluorescence of **1**–**17** ranges from violet to yellow-green.

Interestingly, the trend for the fluorescence maxima (λ_{max}^{fl}) in **1**–**6** was found to be different from that for their longest absorption maxima (λ_{max}^{abs}). Thus, the λ_{max}^{fl} values of **4**–**6** are red-shifted relative to that of **1**, whereas the values of **2** and **3**

DOI: 10.1021/acs.joc.5b01409
J. Org. Chem. 2015, 80, 9076–9090

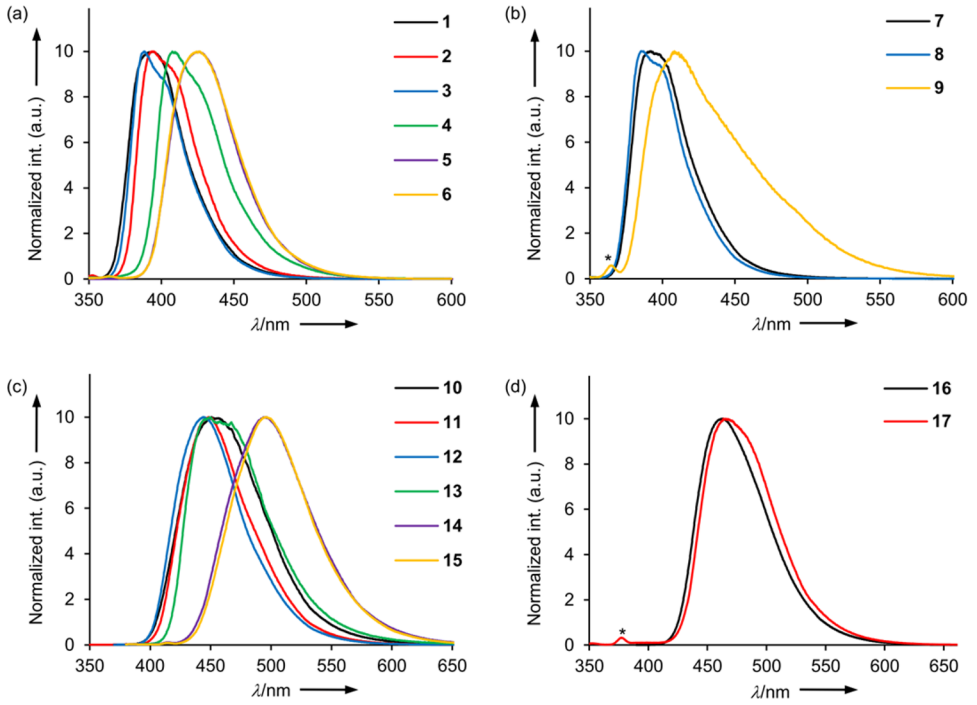

Figure 4. Fluorescence spectra of (a) **1**–**6**, (b) **7**–**9**, (c) **10**–**15**, and (d) **16** and **17** in THF at RT. The excitation wavelengths λ_{ex} = 320 nm for **1**–**3**, **7**, and **8**; 330 nm for **6**, **9**, and **13**; 340 nm for **17**; 360 nm for **4**, **5**, and **10**–**12**; 370 nm for **14** and **15**; and 380 nm for **16**. The spectra of **5** and **6** are highly overlapped accidentally. The peaks attributed to Raman scattering are labeled with an asterisk.

are not (Figure 4a). This stands in contrast to the finding that the longest λ_{max}^{abs} values of **2**–**6** are red-shifted relative to that of **1** regardless of the substituents at the 2-position of the pyrimidine moiety. Accordingly, as compared to the Stokes shift ($\Delta\nu_{fl-abs}$) for **1**, compounds **2** and **3** display the small $\Delta\nu_{fl-abs}$ values, and **4**–**6** show the large values. Under the assumption that the structural changes of the molecule between the ground and excited states in **1**–**6** are similar to each other, these results suggest that their polarity difference between the ground and excited states depends on the substituent on the pyrimidine moiety, and thereby **1**–**6** differ in the extent of stabilization from the Frank–Condon states caused by solvent relaxation. Thus, it seems that in general the polarity difference between the ground and excited states decreases with regard to the electron-donating substituents, while it increases with regard to the electron-withdrawing substituents. We note that the $\Delta\nu_{fl-abs}$ value for the strongly electron-donating piperidyl-substituted **4** is larger than that for **1**, the reason for which may be that the electronic structure of **4** is largely different from those of **1**–**3**, **5**, and **6** (*vide supra*).

The shape of the fluorescence spectra of **7** and **8** is nearly identical to that of **1** and **3**, respectively, and both λ_{max}^{fl} and $\Delta\nu_{fl-abs}$ values of **7** and **8** are similar to those of **1** and **3**, respectively (Figure 4b). This observation clearly confirms that the electronic structures in the excited state as well as the ground state of **7** and **8** resemble those of the corresponding **1** and **3**. Compound **9** features the highly broadened fluorescence spectrum as compared to **6**, and the tail of the spectrum of **9** reaches into about 600 nm, indicating that **6** and **9** differ in the electronic structures in the excited state.

Similar to the change of the longest λ_{max}^{abs} values of **1**–**6** and **10**–**15** as described above, the λ_{max}^{fl} values of **10**–**15** are red-shifted compared to those of the corresponding **1**–**6** by 37–70 nm (Figure 4c). Compounds **10**–**15** feature larger $\Delta\nu_{fl-abs}$ values than the corresponding **1**–**6**, suggesting that the ethynylene spacers enhance the polarity difference between the ground and excited states (*vide infra*). In the series of **10**–**15**, as is the case with **1**–**6**, the electron-withdrawing substituents on the pyrimidine moiety result in the pronounced red-shifts of the λ_{max}^{fl} values and thus increase the $\Delta\nu_{fl-abs}$ values, while the electron-donating substituents decrease the $\Delta\nu_{fl-abs}$ values. As shown in Figure 4d, the λ_{max}^{fl} values of **16** and **17** having vinylene spacers are further red-shifted relative to those of **10** by 12 nm and **11** by 15 nm, respectively, which is consistent with the finding that **16** and **17** display the red-shifted λ_{max}^{abs} values compared to **10** and **11**, respectively.

We determined the absolute fluorescence quantum yields (Φ_f) of **1**–**17** in THF (Table 1). The Φ_f values of **1**–**17** vary from 0.08 to 0.74. The important effects of substituents and spacers on the Φ_f values are summarized as follows: (1) The electron-withdrawing substituents tend to ensure higher Φ_f values than the electron-donating substituents (0.44 (**1**), 0.23 (**2**), 0.61 (**5**)). (2) The introduction of the ethynylene spacer increases the Φ_f values, whereas that of the vinylene spacer decreases the values (0.74 (**10**), 0.25 (**16**)). (3) The attachment of the benzene ring at the 2-position of the pyrimidine ring is ineffective in increasing the Φ_f values. Rather, **9** displays the extremely low Φ_f value of 0.08. (4) The piperidyl substituent markedly decreases the Φ_f values (0.15 (**4**), 0.21 (**13**)), which may be attributed to the lone pair on piperidyl nitrogen atoms.

To obtain further insight into the relationship between the structure and photophysical properties of **1**–**17**, we determined the fluorescence lifetimes (τ_f) with the time-correlated single-photon counting method and calculated the radiative (k_r) and nonradiative (k_{nr}) decay constants from the singlet excited state, based on the equations $k_r = \Phi_f/\tau_f$ and $k_{nr} = (1 - \Phi_f)/\tau_f$ (Table 1). The emission decay profiles of **1**–**15** were numerically fitted by single exponential kinetics, whereas those of **16** and **17** were not: reliable k_r and k_{nr} values for **16**

DOI: 10.1021/acs.joc.5b01409
J. Org. Chem. 2015, 80, 9076–9090

and **17** were not obtained. This implies that the photoisomerization in **16** and **17** occurs during the fluorescence lifetime measurements. In the series **1**–**6**, the substituents affect the values of k_{nr} more than k_r. For example, the k_{nr} value for **2** is almost twice as large as that for **1**, whereas the k_r value for **2** is comparable to that for **1**. This confirms that the lower Φ_f value for **2** as compared to that for **1** is attributed to the faster nonradiative process from the singlet excited state in **2**. Exceptionally, the k_r value for **4** is almost one-half the values for **1**–**3**, **5**, and **6**. Thus, the reason for the significantly low Φ_f value of **4** relative to **1**–**3**, **5**, and **6** is that the piperidyl substituent in **4** not only accelerates the nonradiative process but also decelerates the radiative process. The values of both k_r and k_{nr} for **7** and **8** are comparable to those for **1** and **2**, respectively. Compounds **6** and **9** show similar k_{nr} values; however, **9** displays the extremely low k_r value of 1.5×10^7 s^{-1} compared to that for **6** (24×10^7 s^{-1}). The k_r value for **9** is the lowest value in the present study. This demonstrates that the fluorescence quenching in **9** results from its significantly slow radiative process. The k_{nr} values for **10**–**15** are exclusively lower than those for the corresponding **1**–**6**. This clearly indicates that the ethynylene spacers effectively suppress the nonradiative process, leading to the enhancement of the fluorescence efficiency in **10**–**15**. It is worth stating that the remarkably higher Φ_f values of **10**–**12** as compared to the corresponding **1**–**3** also derive from the promotion of the radiative process together with the suppression of the nonradiative process in the former.

To investigate the solvent effects on the photophysical properties, we measured the UV–vis and fluorescence spectra in various media from nonpolar to polar solvents, namely, toluene, EtOAc, CH_2Cl_2, and DMF. Notably, pronounced positive fluorescence solvatochromism depending on the solvent polarity is observed for **1**–**17** (Figure 5 and Figures S4–S9), whereas their UV–vis spectra exhibit almost no solvatochromism ($\Delta\lambda_{max}^{abs}$ < 8 nm). As a typical example, Figure 5 shows the fluorescence spectra of **14** in various solvents. Upon increasing the solvent polarity from toluene to DMF,[29] the longest λ_{max}^{fl} values of **14** are markedly red-shifted (447 nm in toluene, 550 nm in DMF), and the spectra are broadened. This clearly indicates that **1**–**17** have a more polar electronic structure in the excited state, namely, an intramolecular CT state, than in the ground state. We measured the Φ_f values of **1**–**17** in various solvents (Tables S1–S4) but could not find any general relationship between the solvent polarity and their Φ_f values. It is noteworthy that a number of carbazole–pyrimidine conjugates in the present study display the Φ_f values more than 0.5 even in polar DMF; the fluorescence quenching in polar solvents is observed in many push–pull fluorophores.

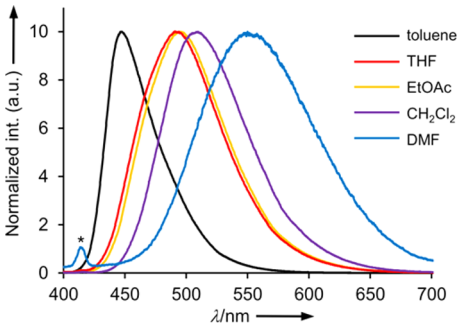

Figure 5. Fluorescence spectra of **14** in various solvents at RT. λ_{ex} = 370 nm. The peak attributed to Raman scattering is labeled with an asterisk.

The Reichardt equation allows a quantitative treatment of the observed fluorescence solvatochromism for **1**–**17**.[30] The solvent-dependent Stokes shifts ($\Delta\nu_{fl-abs}$) were plotted against the normalized solvent polarity (E_T^N) of Reichardt according to

$$\Delta\nu_{fl-abs} = mE_T^N + \text{constant (Reichardt equation)}$$

where m represents the slope of the linear relationship corresponding to the above equation. Consequently, the spectral shifts of the emission were found to follow a linear trend in general (Figures S10 and S11), thus confirming the ICT emission.[31] The change in dipole moment ($\Delta\mu_{e-g}$) from the ground to the excited state can be calculated with the following equation

$$\Delta\mu_{e-g} = (81m/(11\,307.6(6.2/a)^3))^{1/2}$$

where a represents the Onsager radius of the solute. Therefore, assuming that the cavity radii of molecules is similar, the steep slope in the Reichardt plot, that is, a high m value, provides high $\Delta\mu_{e-g}$ values, namely, the large difference of the dipole moment of molecules from the ground to the excited state. Interestingly, the slope in the Reichardt plot for **10** is apparently steeper than that for **1** and **16** (Figure 6), and thereby the $\Delta\mu_{e-g}$ value for **10** should be larger than that for **1** and **16**. This indicates that the ethynylene spacers bring about the large difference of the dipole moment of molecules relative to the vinylene spacers.

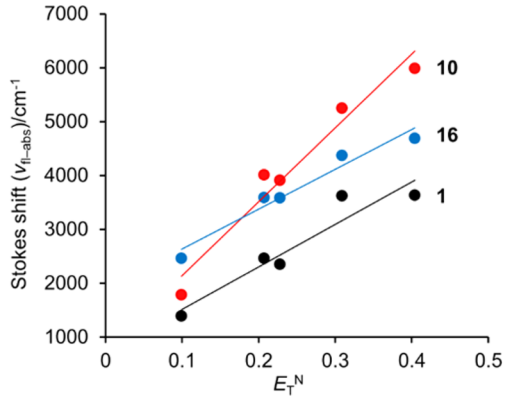

Figure 6. Reichardt plots for **1**, **10**, and **16**. The goodness of fit parameter r^2 = 0.91 (**1**), 0.96 (**10**), and 0.96 (**16**).

Photophysical Properties upon Addition of TFA. Some pyrimidine derivatives are known to function as colorimetric and/or fluorescent pH sensors due to the basic character of the nitrogen atoms of the pyrimidine ring,[12c–e] and hence we subjected **1** to titration-based analysis. Here, UV–vis and fluorescence spectral changes of **1** upon addition of trifluoroacetic acid (TFA) in CH_2Cl_2 were monitored (Figure 7). Upon addition of TFA, the absorption maxima at 286, 349, and 360 nm were seen to decrease, and a new absorption around 450 nm was found to increase (Figure 7a). The fluorescence emission at 417 nm of **1** was found to decrease upon addition of TFA, and a new fluorescence around 530 nm was seen to increase (Figure 7b). The observed spectral changes indicated the formation of the protonated species of **1**.[32] Almost no spectral change was observed by addition of more than 6300

DOI: 10.1021/acs.joc.5b01409
J. Org. Chem. 2015, 80, 9076–9090

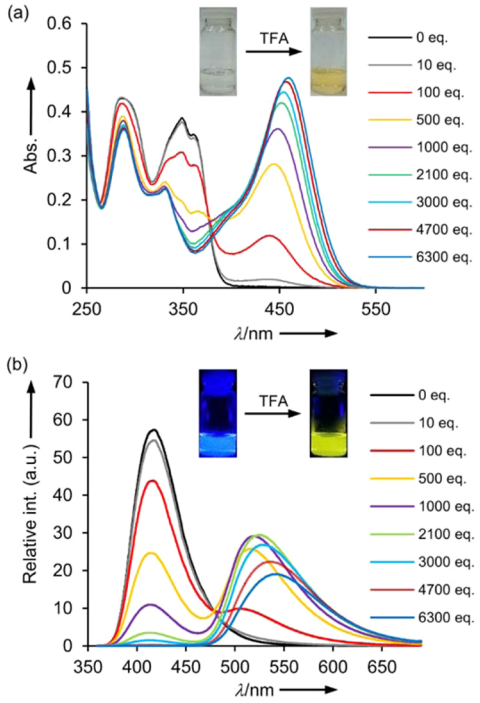

Figure 7. (a) Electronic absorption and (b) fluorescence spectral change of **1** in CH_2Cl_2 (1×10^{-5} mol L^{-1}) upon addition of TFA at RT. λ_{ex} = 350 nm. The inset shows the color changes upon addition of 10 000 equiv of TFA.

equiv of TFA: the absorbance hardly changed in the UV−vis spectra, and the original emission at 417 nm was completely quenched in the fluorescence spectra.[33] The red-shift of the absorption is explained by the effective lowering of the LUMO level compared to the HOMO level,[34] namely, the decrease in the HOMO−LUMO gap by protonation of the pyrimidine ring. Accordingly, the CH_2Cl_2 solution of **1** underwent a significant color change from colorless to yellow upon addition of an excess amount of TFA, and the fluorescence color of the solution was also seen to change from sky blue to yellow. Neutralization with Et_3N almost regenerated the original UV−vis and fluorescence spectra (Figure S12).

We investigated the changes of the UV−vis and fluorescence spectra and the Φ_f values of **2**−**9** together with **1** upon addition of 10 000 equiv of TFA in CH_2Cl_2 at 1×10^{-5} mol L^{-1} (Table 2). As is the case with **1**, the CH_2Cl_2 solutions of **2**−**4** and **7**−**9** underwent significant spectral changes in the presence of TFA, clearly indicating the formation of protonated species (Figures S13−S15).[35] In the UV−vis spectra, the original absorptions around 350 nm decrease, and new absorptions around 450 nm appear. Moreover, in the fluorescence spectra, the original fluorescence emission bands around 410 nm disappear, and new emission bands around 510−570 nm appear. The clear relationship between the change of the Φ_f values and the substituents on the pyrimidine moiety was not observable. Thus, the Φ_f values of **1** and **7** decreased after protonation, and surprisingly those of **2** and **4** increased. The values of **3**, **8**, and **9** varied only slightly.

In contrast, **5** and **6** afforded almost no UV−vis spectral changes upon addition of an excess amount of TFA (Figure S14); the new absorptions for **5** and **6** around 530 nm are extremely weak as compared to those of **1**−**4** and **7**−**9** (Figure S14). This indicated the ineffective protonation of **5** and **6** as

Table 2. Photophysical Properties of 1−9 in Dichloromethane (1×10^{-5} mol L^{-1}) in the Presence and Absence of TFA (10 000 equiv)[a]

	λ_{max}^{abs}/nm	λ_{max}^{fl}/nm	Φ_f[b]
1	463 (360)	546[c] (414[c])	0.28 (0.75)
2	471 (370)	549[c] (411[c])	0.53 (0.31)
3	473 (366)	543[c] (408[c])	0.63 (0.69)
4	445 (371)	513[d] (414[d])	0.46 (0.15)
5	533 (384)	437[d] (437[d])	0.15 (0.72)
6	523 (381)	435[d] (435[d])	0.16 (0.29)
7	484 (363)	552[c] (405[c])	0.43 (0.65)
8	477 (364)	548[e] (405[e])	0.48 (0.42)
9	477 (365)	574[c] (420[c])	0.08 (0.11)

[a]The values in the absence of TFA are in the parentheses. [b]Absolute fluorescence quantum yields determined by an integrating sphere system. [c]λ_{ex} = 350 nm. [d]λ_{ex} = 360 nm. [e]λ_{ex} = 340 nm.

compared to **1**−**4** and **7**−**9**: the electron-withdrawing SO_2Me and CN groups in **5** and **6**, respectively, should decrease the basicity of the pyrimidine nitrogen atoms.[36] The fluorescence emission spectra of **5** and **6** were suppressed monotonically and thus the Φ_f values of **5** and **6** decreased by addition of TFA (Table 2): a red-shifted emission band was not observed for **5** and **6**. This finding suggests the nonfluorescent nature of the protonated species of **5** and **6**.

Electrochemical Properties. We first performed cyclic voltammetry (CV) experiments on **1**−**17** in *o*-DCB (0.1 mol L^{-1} *n*-Bu_4NPF_6, standard Fc^+/Fc) to investigate their electrochemical properties. Compounds **1**−**13**, **16**, and **17** underwent carbazole-centered two $1e^-$ oxidation steps, while **14** and **15** exhibited one $2e^-$ oxidation step (Figures S16 and S17). Compounds **2**, **5**, **6**, and **9**−**17** experienced a pyrimidine-centered one $1e^-$ reduction step; however, the reduction behavior for **1**, **3**, **4**, **7**, and **8** was not clear: the substantial peak amplitude was observed around −2.6 V. This suggests that the anionic species for **1**, **3**, **4**, **7**, and **8** rapidly decomposed upon electrochemical reduction due to the instability and/or their reduction potentials are outside the potential window.

The redox behaviors of **1**−**17** were further investigated by differential pulse voltammetry (DPV) in *o*-DCB (Table 3), because DPV offers better sensitivity than CV and leads to steeper peak onsets due to the sharper current response. All the compounds underwent the oxidation processes, and the compounds except for **4** experienced the reduction processes (Figures S18 and S19). The fact that the reduction process was not observed for **4** is attributable to the strongly electron-donating piperidyl group, which should decrease the electron-withdrawing ability of the pyrimidine ring substantially. It is likely that the functional groups on the pyrimidine ring in **1**−**6** affect the reduction potentials (E_{red}) relative to the oxidation potentials (E_{ox}). Interestingly, the reductions are apparently facilitated for **2** and **3** compared to **1** (−2.73 V (**1**), −2.55 V (**2**), −2.68 V (**3**)), indicating that both SMe and OMe groups in **2** and **3**, respectively, function as an electron-withdrawing group. When compared to the E_{red} values of **2** and **3**, those of **5** and **6** are anodically shifted due to the strongly electron-withdrawing ability of SO_2Me and CN groups. Noticeably, the substituent effects on the E_{red} values observed in **1**−**6** hold true for **10**−**15**.

Compounds **7**, **8**, and **9** are oxidized at almost the same potential as those of the corresponding **1**, **3**, and **6**. Additionally, the E_{red} values of **8** and **9** are similar to those of

DOI: 10.1021/acs.joc.5b01409
J. Org. Chem. 2015, 80, 9076−9090

Table 3. Oxidation and Reduction Potentials of 1−17 by DPV (0.1 mol L^{-1} n-Bu_4NPF_6) in o-DCB,[a] Theoretically Calculated HOMO and LUMO Levels,[b] and Electrochemical (ΔE_{redox}),[c] Theoretical (ΔE_{calcd}),[d] and Optical Gaps (ΔE_{opt})[e]

	E_{ox}/V	E_{red}/V	HOMO[b]/eV	LUMO[b]/eV	ΔE_{redox}/V	ΔE_{calcd}/eV	ΔE_{opt}/eV
1	0.75, 0.96	−2.73	−5.58	−1.54	3.48	4.04	3.44
2	0.73, 0.93	−2.55	−5.57	−1.59	3.28	3.98	3.34
3	0.72, 0.92	−2.68	−5.53	−1.51	3.40	4.02	3.39
4	0.63, 0.88	*f*	−5.34	−1.28	*g*	4.06	3.38
5	0.78, 0.94	−2.28	−5.79	−2.01	3.06	3.78	3.25
6	0.79, 0.94	−2.30	−5.79	−1.96	3.09	3.83	3.25
7	0.73, 0.92	−2.60	−5.58	−1.52	3.33	4.06	3.41
8	0.72, 0.92	−2.72	−5.51	−1.45	3.44	4.06	3.40
9	0.73, 0.92	−2.30	−5.74	−2.08	3.03	3.66	3.38
10	0.80, 0.93	−2.21	−5.60	−2.00	3.01	3.60	3.25
11	0.77, 0.88	−2.11	−5.59	−2.04	2.88	3.55	3.13
12	0.77, 0.87	−2.16	−5.56	−1.96	2.93	3.60	3.20
13	0.72, 0.87	−2.36	−5.37	−1.78	3.08	3.59	3.16
14	0.82, 0.90	−1.84	−5.78	−2.45	2.66	3.33	3.04
15	0.84, 0.88	−1.86	−5.78	−2.39	2.70	3.39	3.02
16	0.55, 0.78	−2.26	−5.38	−2.00	2.81	3.38	3.12
17	0.55, 0.82	−2.18	−5.38	−2.04	2.73	3.34	3.05

[a]All potentials are given versus the Fc^+/Fc couple used as external standard. Pulse width of 100 ms in a period of 200 ms. [b]B3LYP/6-311G(d,p)//B3LYP/6-31G(d). [c]Electrochemical gap, ΔE_{redox}, is defined as the potential difference between the first oxidation potential and the first reduction potential. [d]Theoretical gap, ΔE_{calcd}, is defined as the energy difference between the HOMO and the LUMO calculated by the DFT method. [e]Optical gap, ΔE_{opt}, is defined as the energy corresponding to the λ_{max}^{abs} in THF. [f]Not observed. [g]Not determined.

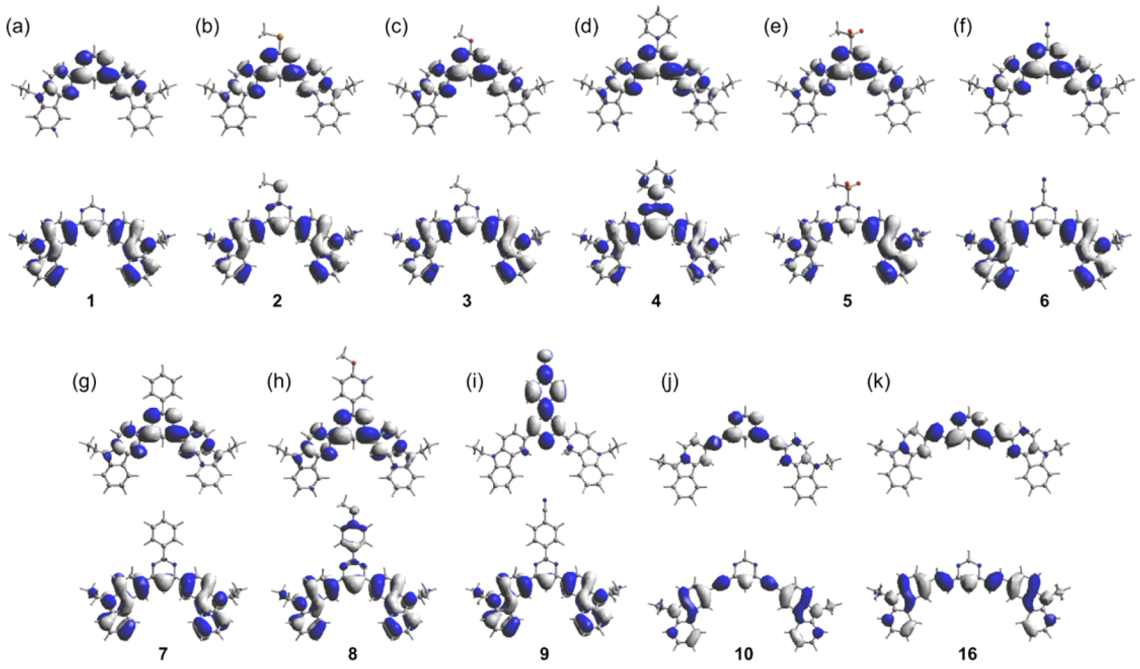

Figure 8. FMO plots (B3LYP/6-311G(d,p)//B3LYP/6-31G(d)) of (a) **1**, (b) **2**, (c) **3**, (d) **4**, (e) **5**, (f) **6**, (g) **7**, (h) **8**, (i) **9**, (j) **10**, and (k) **16**. The lower plots represent the HOMOs, and the upper plots represent the LUMOs. FMO plots of **11**−**15** and **17** are shown in Figure S25 in the Supporting Information.

3 and **6**, respectively. These findings support the negligible effect of the benzene ring at the 2-position of the pyrimidine moiety on both the HOMO and LUMO levels; however, the reason for the positive shift of the E_{red} value of **7** relative to **1** by 130 mV is unclear at present.

Compounds **10**−**17** with π-spacers displayed remarkable anodic shifts of the E_{red} values (−2.36 to −1.84 V) relative to those (−2.73 to −2.28 V) of the corresponding **1**−**6**, demonstrating that both the ethynylene and vinylene spacers substantially lower the LUMO levels. The E_{ox} values of **10**−**15** are positively shifted compared to those of the corresponding **1**−**6** by 40−90 mV, while the values of **16** and **17** are negatively shifted relative to those of **1** by 200 mV and **2** by 180 mV, respectively. Hence, the ethynylene spacer lowers the HOMO levels together with the LUMO levels, whereas the vinylene spacer elevates the HOMO levels.[37]

We calculated the differences between the E_{ox} and E_{red} values determined by DPV analyses, namely, the electrochemical HOMO−LUMO gaps (ΔE_{redox}) of the compounds except for **4** (Table 3). A plot of the optical gaps (ΔE_{opt}), calculated from

DOI: 10.1021/acs.joc.5b01409
J. Org. Chem. 2015, 80, 9076−9090

the longest λ_{max}^{abs} values in THF, against the ΔE_{redox} values shows substantial deviation of **9** and **13** from a linear correlation (Figure S20a in the Supporting Information). This suggests that the frontier molecular orbitals (FMOs) responsible for the optical gaps of **9** and **13** are different from those for the electrochemical gaps and/or the distribution of FMOs involved with the electronic transition in the longer wavelength region of **9** and **13** is distinctively different from that of other compounds (*vide infra*).

Quantum Chemical Calculations. To obtain further insight into the electronic properties of **1**−**17**, we performed their geometrical optimization and FMO calculations.[38] We used the molecular structures of **1**−**17** with the two-*cisoid* conformation as the initial structures for the geometrical optimization due to the following reasons: (1) As determined by X-ray diffraction analyses, **3** and **6** adopt the two-*cisoid* conformation in the solid state. (2) The dipole moments of the molecules with the two-*cisoid* conformation are smaller than those with the two-*transoid* or the *cisoid*−*transoid* conformation regardless of the substituent at the 2-position of the pyrimidine ring (Figures S21−S23 in the Supporting Information). The FMO plots and the HOMO and LUMO levels were obtained by the single-point calculations at the B3LYP/6-311G(d,p)//B3LYP/6-31G(d) level of theory. The results are summarized in Table 3, and the HOMOs and LUMOs of **1**−**17** are shown in Figure 8 and Figure S25. The geometrical optimization suggests that the conjugated backbone of **1**−**9** presents a minor deviation from planarity, and thus the dihedral angles of the pyrimidine and carbazole moieties in **1**−**9** are calculated to be ca. 13° due to the steric repulsion of the hydrogen atoms at the 5-position of pyrimidine and the 4-position of carbazole. In contrast, **10**−**17** have an almost completely planar structure owing to the release of the above-mentioned steric repulsion by π-spacers.[39] Except for **4**, **9**, and **13**, the HOMOs and LUMOs of the molecules are mainly localized in the carbazole and pyrimidine moieties, respectively. The HOMOs of **4** and **13** are delocalized over almost the whole molecular framework: they have large contribution from the pyrimidine and piperidine moieties as well as the carbazole moieties. This apparently visualizes the pronounced electronic perturbation of the piperidyl group in **4** and **13**. The LUMO density of **9** is fully localized in the pyrimidine and cyanophenyl moieties: the LUMO of **9** has almost no contribution from the carbazole moiety. In **10**−**17**, the ethynylene and vinylene spacers contribute to both the HOMOs and LUMOs, clearly indicating the efficient extension of π-conjugation as a result of the introduction of spacers. A plot of HOMO−LUMO gaps (ΔE_{calcd}) by DFT calculations against the ΔE_{redox} values shows a linear correlation (Figure S20b). The ΔE_{calcd} values are larger than the ΔE_{redox} values by 0.5−0.7 eV, probably reflecting that the calculations were performed under the gas-phase conditions.

It is interesting to note that the electron density distributions in the LUMOs of the compounds except for **9** are similar to each other, and the 2-position of the pyrimidine moiety lies in the nodal plane of the LUMOs. This finding suggests that the inductive effect of the substituents at the 2-position of pyrimidine on the LUMOs exceeds the resonance effect, which rationalizes the fact that the E_{red} values of **2**, **3**, and **7** with SMe, OMe, and phenyl groups, respectively, are positively shifted relative to that of **1**.[40]

We carried out the time-dependent (TD) DFT calculations for **1**−**17** at the TD-B3LYP/6-31G(d)//B3LYP/6-31G(d) level to study their electronic transitions (Table S6 in the Supporting Information). Except for **9**, the absorption maxima in the low-energy region are mainly attributed to the HOMO−LUMO transitions from the carbazole donor to the pyrimidine acceptor moieties with ICT character. On the other hand, the absorption maximum of **9** is related to the HOMO−LUMO + 1 transition, and the HOMO−LUMO transition is forbidden in **9**,[41] which may be one of the reasons for its broad emission bands (*vide supra*) and low Φ_f values (0.07−0.34). The electronic distribution of the LUMO + 1 of **9** resembles that of the LUMOs of **1**−**8** (Figure S24), and hence the HOMO−LUMO + 1 transition of **9** can also be recognized as the ICT transition.[42] In general, the longest λ_{max}^{abs} values estimated by the calculations are in good agreement with those obtained by the experiments. Thus, the calculations reproduced well the experimentally observed findings that the substituents at the 2-position of pyrimidine and the π-spacers between the carbazole and pyrimidine moieties lead to the red-shifts of the longest λ_{max}^{abs} values.

CONCLUSION

We have synthesized a series of carbazole−pyrimidine conjugates **1**−**17** by means of the Pd-catalyzed cross-coupling, oxidation, and nucleophilic aromatic substitution (S_NAr) reactions. The X-ray crystal structures of **3**, **6**, **11**, and **14** revealed that the carbazole and pyrimidine moieties are effectively conjugated, and the electron-donating carbazole moiety tends to overlap with the electron-accepting pyrimidine moiety in the solid state. The properties of **1**−**17** were approached by electronic absorption and fluorescence spectral measurements, DPV, and DFT calculations, and the effects of substituents at the 2-position of the pyrimidine ring and π-spacers between the carbazole and pyrimidine moieties on their properties were revealed. Their electronic absorption spectra were dominated by ICT absorptions in the UV−vis region of 320−420 nm. The electron-withdrawing substituents and the vinylene spacer relative to the electron-donating substituents and the ethynylene spacer, respectively, lead to distinctive red-shifts of the longest λ_{max}^{abs} values. Compounds **1**−**17** essentially exhibit strong fluorescence in violet, blue, green, or yellow-green color with large Stokes shifts depending on the solvent polarity characteristic of ICT fluorophores. Most of **1**−**9** display pronounced change in optical and fluorescence properties upon addition of TFA, and some of the compounds show remarkable fluorescence even when they are protonated. The compounds presented herein displayed electrochemical amphoterism in *o*-DCB except for **4**. Their electron-accepting ability can be altered by the inductive effects of substituents on the pyrimidine ring. The ethynylene spacer lowers both the HOMO and LUMO levels, whereas the vinylene spacer elevates the HOMO level and lowers the LUMO level. We expect that the adjustable electronic absorption, fluorescence, and electrochemical properties and the established and efficient methodologies for derivatization, together, make carbazole−pyrimidine conjugates promising candidates as photophysically and electrochemically active functional materials. Further structural functionalization of mixed π-systems comprising carbazole and pyrimidine is currently underway in our group.

EXPERIMENTAL SECTION

Preparation of 9-Ethyl-3-[6-(9-ethyl-9*H*-carbazol-3-yl)-pyrimidin-4-yl]-9*H*-carbazole (1). A mixture of 4,6-dichloropyrimidine (39 mg, 0.26 mmol) and **18** (0.21 g, 0.65 mmol) in DME (10

DOI: 10.1021/acs.joc.5b01409
J. Org. Chem. 2015, 80, 9076−9090

mL) and aqueous $NaHCO_3$ (2 mol L^{-1}, 3 mL) was bubbled with argon for 0.5 h. $[Pd(PPh_3)_4]$ (18 mg, 15 μmol) was added to the mixture, and the resulting mixture was refluxed for 15 h under argon atmosphere. After addition of water (10 mL), the organic phase was separated, and the aqueous phase was extracted with toluene (10 mL × 3). The combined organic phase was washed with water (10 mL × 2), dried over anhydrous $MgSO_4$, and concentrated under reduced pressure. The residue was purified by column chromatography (silica gel, toluene/EtOAc) to give **1** (0.10 g, 88%) as white solids. Mp 176−177 °C. ^{1}H NMR (500 MHz, $CDCl_3$): δ 9.36 (1H, s), 8.93 (2H, s), 8.27−8.24 (4H, m), 8.17 (1H, s), 7.50 (2H, t, *J* = 7.2 Hz), 7.41 (2H, d, *J* = 8.6 Hz), 7.37 (2H, d, *J* = 8.2 Hz), 7.32 (2H, t, *J* = 7.2 Hz), 4.27 (4H, q, *J* = 7.2 Hz), 1.41 (6H, t, *J* = 7.2 Hz). ^{13}C NMR (125 MHz, $CDCl_3$): δ 164.7, 158.9, 141.6, 140.5, 127.8, 126.2, 124.8, 123.4, 123.2, 120.8, 119.7, 119.5, 111.4, 108.8, 108.6, 37.6, 13.8. UV−vis (CH_2Cl_2): λ_{max}^{abs} (ε) 360 (35 400), 348 (38 600), 286 nm (42 400). HR-ESI-TOF-MS: *m*/*z* calcd for $C_{32}H_{27}N_4^+$ 467.2236, found 467.2226 [(M + H)$^+$].

Preparation of 9-Ethyl-3-[6-(9-ethyl-9*H*-carbazol-3-yl)-2-(methylsulfanyl)pyrimidin-4-yl]-9*H*-carbazole (2). A mixture of 4,6-dichloro-2-(methylsulfanyl)pyrimidine (0.29 g, 1.5 mmol) and **18** (1.2 g, 3.7 mmol) in DME (20 mL) and aqueous $NaHCO_3$ (2 mol L^{-1}, 5 mL) was bubbled with argon for 0.5 h. $[Pd(PPh_3)_4]$ (0.10 g, 90 μmol) was added to the mixture, and the resulting mixture was refluxed for 15 h under argon atmosphere. After addition of water (10 mL), the organic phase was separated, and the aqueous phase was extracted with toluene (10 mL × 3). The combined organic phase was washed with water (10 mL × 2), dried over anhydrous $MgSO_4$, and concentrated under reduced pressure. The residue was purified by column chromatography (silica gel, toluene/hexane = 6:1) to give **2** (0.72 g, 95%) as white solids. Mp 208−211 °C. ^{1}H NMR (500 MHz, $CDCl_3$): δ 8.97 (2H, d, *J* = 1.8 Hz), 8.38 (2H, dd, *J* = 8.6, 1.8 Hz), 8.26 (2H, d, *J* = 7.5 Hz), 8.01 (1H, s), 7.54−7.51 (4H, m), 7.46 (2H, d, *J* = 8.1 Hz), 7.32 (2H, t, *J* = 7.5 Hz), 4.43 (4H, q, *J* = 7.5 Hz), 2.83 (3H, s), 1.49 (6H, t, *J* = 7.5 Hz). ^{13}C NMR (125 MHz, $CDCl_3$): δ 172.0, 164.9, 141.6, 140.5, 127.9, 126.1, 125.1, 123.34, 123.20, 120.7, 119.8, 119.4, 108.8, 108.5, 106.9, 37.7, 14.4, 13.8. UV−vis (CH_2Cl_2): λ_{max}^{abs} (ε) 370 (37 300), 350 (33 900), 294 nm (48 000). HR-ESI-TOF-MS: *m*/*z* calcd for $C_{33}H_{29}N_4S^+$ 513.2107, found 513.2117 [(M + H)$^+$].

Preparation of 9-Ethyl-3-[6-(9-ethyl-9*H*-carbazol-3-yl)-2-methoxypyrimidin-4-yl]-9*H*-carbazole (3). To a suspension of NaH (60%, 10 mg, 0.25 mmol) in DMF was added methanol (0.10 mL, 2.5 mmol) at room temperature under argon atmosphere. Then, **5** (30 mg, 55 μmol) was added to the mixture, and the resulting mixture was stirred at 60 °C for 1.5 h. After addition of water (10 mL), the aqueous phase was extracted with CH_2Cl_2 (10 mL × 3). The organic phase was washed with water (10 mL × 3), dried over anhydrous $MgSO_4$, and concentrated under reduced pressure. The residue was purified by column chromatography (silica gel, toluene) to give **3** (28 mg, 85%) as white solids. Mp 190−192 °C. ^{1}H NMR (500 MHz, $CDCl_3$): δ 9.00 (2H, s), 8.37 (2H, d, *J* = 8.6 Hz), 8.26 (2H, d, *J* = 7.7 Hz), 7.99 (1H, s), 7.54−7.48 (4H, m), 7.44 (2H, d, *J* = 8.2 Hz), 7.32 (2H, t, *J* = 7.7 Hz), 4.39 (4H, q, *J* = 7.4 Hz), 4.27 (3H, s), 1.47 (6H, t, *J* = 7.4 Hz). ^{13}C NMR (125 MHz, $CDCl_3$): δ 167.3, 166.2, 141.7, 140.6, 128.0, 126.2, 125.2, 123.43, 123.37, 120.9, 120.0, 119.6, 108.9, 108.6, 105.5, 54.8, 37.8, 13.9. UV−vis (CH_2Cl_2): λ_{max}^{abs} (ε) 369 (36 800), 351 (31 900), 282 nm (43 300). HR-ESI-TOF-MS: *m*/*z* calcd for $C_{33}H_{29}N_4O^+$ 497.2341, found 497.2328 [(M + H)$^+$].

Preparation of 9-Ethyl-3-[6-(9-ethyl-9*H*-carbazol-3-yl)-2-(piperidin-1-yl)pyrimidin-4-yl]-9*H*-carbazole (4). A mixture of **5** (32 mg, 59 μmol) and piperidine (34 μL, 0.34 mmol) in 1,4-dioxane (5 mL) was heated at 50 °C for 20 h under argon atmosphere. After addition of water, the organic phase was separated, and the aqueous phase was extracted with EtOAc (10 mL × 3). The combined organic phase was washed with water (10 mL × 3), dried over anhydrous $MgSO_4$, and concentrated under reduced pressure. The residue was purified by column chromatography (silica gel, toluene) to give **4** (30 mg, 93%) as white solids. Mp 129−131 °C. ^{1}H NMR (500 MHz, $CDCl_3$): δ 8.96 (2H, s), 8.40 (2H, d, *J* = 8.4 Hz), 8.29 (2H, d, *J* = 7.6 Hz), 7.66 (1H, s), 7.54−7.50 (4H, m), 7.46 (2H, d, *J* = 8.4 Hz), 7.32 (2H, t, *J* = 7.6 Hz), 4.42 (4H, q, *J* = 7.2 Hz), 4.15 (4H, brs), 1.79 (6H, brs), 1.48 (6H, t, *J* = 7.2 Hz). ^{13}C NMR (125 MHz, $CDCl_3$): δ 165.5, 162.6, 141.4, 140.5, 129.7, 126.0, 125.2, 123.46, 123.29, 120.8, 119.6, 119.3, 108.8, 108.4, 100.8, 45.1, 37.8, 26.1, 25.3, 13.9. UV−vis (CH_2Cl_2): λ_{max}^{abs} (ε) 371 (21 600), 349 (19 600), 328 (24 800), 295 nm (54 600). HR-ESI-TOF-MS: *m*/*z* calcd for $C_{37}H_{36}N_5^+$ 550.2971, found 550.2961 [(M + H)$^+$].

Preparation of 9-Ethyl-3-[6-(9-ethyl-9*H*-carbazol-3-yl)-2-methanesulfonylpyrimidin-4-yl]-9*H*-carbazole (5). To a solution of **2** (0.10 g, 0.20 mmol) in CH_2Cl_2 (15 mL) was added *m*-chloroperoxybenzoic acid (77%, 0.22 g, 0.98 mmol) at 0 °C. The resulting mixture was warmed to room temperature and stirred for 2 h. After addition of aqueous $Na_2S_2O_3$ (10%, 20 mL), the organic phase was separated, and the aqueous phase was extracted with CH_2Cl_2 (10 mL × 3). The combined organic phase was washed successively with aqueous $Na_2S_2O_3$ (10%, 10 mL × 3) and aqueous $NaHCO_3$ (1 mol L^{-1}, 10 mL × 3), dried over anhydrous $MgSO_4$, and concentrated under reduced pressure. The residue was purified by column chromatography (silica gel, CH_2Cl_2) to give **5** (0.10 g, 97%) as yellow solids. Mp 241−243 °C. ^{1}H NMR (500 MHz, $CDCl_3$): δ 8.87 (2H, s), 8.27 (2H, d, *J* = 8.6 Hz), 8.23 (1H, s), 8.22 (2H, t, *J* = 7.6 Hz), 7.50 (2H, t, *J* = 7.6 Hz), 7.38−7.43 (4H, m), 7.31 (2H, t, *J* = 7.6 Hz), 4.33 (4H, q, *J* = 7.2 Hz), 3.51 (3H, s), 1.45 (6H, t, *J* = 7.2 Hz). ^{13}C NMR (125 MHz, $CDCl_3$): δ 166.2, 142.2, 140.6, 126.5, 126.0, 125.3, 123.5, 123.1, 121.0, 120.3, 119.9, 112.3, 109.0, 108.8, 39.2, 37.8, 13.9 (17 signals out of 18 expected). UV−vis (CH_2Cl_2): λ_{max}^{abs} (ε) 384 (36 500), 353 (25 800), 308 (29 800), 285 nm (30 200). HR-ESI-TOF-MS: *m*/*z* calcd for $C_{33}H_{29}N_4O_2S^+$ 545.2011, found 545.1993 [(M + H)$^+$].

Preparation of 4,6-Bis(9-ethyl-9*H*-carbazol-3-yl)pyrimidine-2-carbonitrile (6). A mixture of **5** (30 mg, 55 μmol) and KCN (8.0 mg, 0.12 mmol) in DMF was heated at 140 °C for 1 h under argon atmosphere. After addition of saturated aqueous $NaHCO_3$ (50 mL), the aqueous phase was extracted with CH_2Cl_2 (10 mL × 3). The organic phase was washed with saturated aqueous $NaHCO_3$ (50 mL × 3), dried over anhydrous Na_2SO_4, and concentrated under reduced pressure. The residue was purified by column chromatography (silica gel, toluene) to give **6** (27 mg, quant) as yellow solids. Mp 219−221 °C. ^{1}H NMR (500 MHz, $CDCl_3$): δ 8.99 (2H, s), 8.40 (1H, s), 8.35 (2H, d, *J* = 8.9 Hz), 8.27 (2H, d, *J* = 7.5 Hz), 7.56−7.54 (4H, m), 7.47 (2H, d, *J* = 8.9 Hz) 7.34 (2H, t, *J* = 7.5 Hz), 4.44 (4H, q, *J* = 7.1 Hz), 1.50 (6H, t, *J* = 7.1 Hz). ^{13}C NMR (125 MHz, $CDCl_3$): δ 165.7, 142.2, 140.7, 126.6, 125.9, 125.0, 123.6, 123.1, 121.00, 120.21, 119.9, 116.9, 112.4, 109.0, 108.9, 37.9, 14.0 (17 signals out of 18 expected). UV−vis (CH_2Cl_2): λ_{max}^{abs} (ε) 381 (38 300), 310 (31 800), 284 nm (29 200). HR-ESI-TOF-MS: *m*/*z* calcd for $C_{33}H_{26}N_5^+$ 492.2188, found 492.2165 [(M + H)$^+$].

Preparation of 9-Ethyl-3-[6-(9-ethyl-9*H*-carbazol-3-yl)-2-phenylpyrimidin-4-yl]-9*H*-carbazole (7). A mixture of **2** (30 mg, 59 μmol) and **19** (20 mg, 0.16 mmol) in DME (5 mL) was bubbled with argon for 0.5 h. Copper(I) thiophene-2-carboxylate (22 mg, 0.12 mmol) and $[Pd(PPh_3)_4]$ (3 mg, 2.6 μmol) were added to the mixture. The resulting mixture was refluxed for 23 h under argon atmosphere. After addition of water (10 mL), the organic phase was separated, and the aqueous phase was extracted with EtOAc (10 mL × 3). The combined organic phase was washed with water (10 mL × 3), dried over anhydrous $MgSO_4$, and concentrated under reduced pressure. The residue was purified by column chromatography (silica gel, toluene/hexane = 2:1) to give **7** (13 mg, 43%) as white solids. Mp 238−239 °C. ^{1}H NMR (500 MHz, $CDCl_3$): δ 9.10 (2H, s), 8.85 (2H, d, *J* = 7.2 Hz), 8.52 (2H, d, *J* = 8.4 Hz), 8.31 (2H, d, *J* = 7.6 Hz), 8.25 (1H, s), 7.61 (2H, t, *J* = 7.2 Hz), 7.53−7.57 (5H, m), 7.47 (2H, d, *J* = 8.4 Hz), 7.32 (2H, t, *J* = 7.2 Hz), 4.44 (4H, q, *J* = 7.2 Hz), 1.50 (6H, t, *J* = 7.2 Hz). ^{13}C NMR (125 MHz, $CDCl_3$): δ 165.1, 164.3, 141.7, 140.6, 138.9, 130.4, 128.78, 128.65, 128.55, 126.2, 125.3, 123.54, 123.42, 120.9, 119.9, 119.5, 109.4, 108.95, 108.79, 37.9, 14.0. UV−vis (CH_2Cl_2): λ_{max}^{abs} (ε) 363 (33 900), 349 (38 000), 298 nm (49 000). HR-ESI-TOF-MS: *m*/*z* calcd for $C_{38}H_{31}N_4^+$ 543.2549, found 543.2579 [(M + H)$^+$].

DOI: 10.1021/acs.joc.5b01409
J. Org. Chem. 2015, 80, 9076−9090

Preparation of 9-Ethyl-3-[6-(9-ethyl-9*H*-carbazol-3-yl)-2-(4-methoxyphenyl)pyrimidin-4-yl]-9*H*-carbazole (8). A mixture of **2** (30 mg, 59 μmol) and **20** (18 mg, 0.12 mmol) in methoxycyclopentane (10 mL) was bubbled with argon for 0.5 h. Copper(I) thiophene-2-carboxylate (22 mg, 0.12 mmol) and [$Pd(PPh_3)_4$] (3 mg, 2.6 μmol) were added to the mixture. The resulting mixture was refluxed for 23 h under argon atmosphere. After addition of water (10 mL), the organic phase was separated, and the aqueous phase was extracted with EtOAc (10 mL × 3). The combined organic phase was washed with water (10 mL × 3), dried over anhydrous $MgSO_4$, and concentrated under reduced pressure. The residue was purified by column chromatography (silica gel, toluene) to give **8** (12 mg, 36%) as white solids. Mp 231−233 °C. ^{1}H NMR (300 MHz, $CDCl_3$): δ 9.09 (2H, d, *J* = 1.6 Hz), 8.81 (2H, d, *J* = 8.9 Hz), 8.51 (2H, dd, *J* = 8.6, 1.6 Hz), 8.31 (2H, d, *J* = 7.6 Hz), 8.20 (1H, s), 7.51−7.57 (4H, m), 7.47 (2H, d, *J* = 7.9 Hz), 7.33 (2H, t, *J* = 7.6 Hz), 7.12 (2H, d, *J* = 8.9 Hz), 4.45 (4H, q, *J* = 7.2 Hz), 3.95 (3H, s) 1.51 (6H, t, *J* = 7.2 Hz). ^{13}C NMR (75 MHz, $CDCl_3$): δ 165.0, 164.1, 161.7, 141.6, 140.6, 131.71, 130.2, 128.9, 126.2, 125.3, 123.51, 123.44, 120.9, 119.8, 119.5, 113.8, 108.93, 108.84, 108.73, 55.5, 37.9, 14.0. UV−vis (CH_2Cl_2): λ_{max}^{abs} (ε) 364 (31 000), 349 (34 400), 298 nm (62 500). HR-ESI-TOF-MS: *m*/*z* calcd for $C_{39}H_{33}N_4O^+$ 573.2654, found 573.2653 [(M + H)$^+$].

Preparation of 4-[4,6-Bis(9-ethyl-9*H*-carbazol-3-yl)-pyrimidin-2-yl]benzonitrile (9). A mixture of **2** (0.23 g, 0.45 mmol) and **21** (0.13 g, 0.89 mmol) in methoxycyclopentane (40 mL) was bubbled with argon for 0.5 h. Copper(I) thiophene-2-carboxylate (0.17 g, 0.89 mmol) and [$Pd(PPh_3)_4$] (23 mg, 20 μmol) were added to the mixture. The resulting mixture was refluxed for 18 h under argon atmosphere. After addition of water (30 mL), the organic phase was separated, and the aqueous phase was extracted with EtOAc (10 mL × 3). The combined organic phase was washed with water (10 mL × 3), dried over anhydrous $MgSO_4$, and concentrated under reduced pressure. The residue was purified by column chromatography (silica gel, toluene) to give **9** (35 mg, 14%) as white solids. Mp 250−252 °C. ^{1}H NMR (400 MHz, $CDCl_3$): δ 9.04 (2H, d, *J* = 1.3 Hz), 8.91 (2H, d, *J* = 8.6 Hz), 8.48 (2H, dd, *J* = 8.6, 1.7 Hz), 8.30 (2H, d, *J* = 7.6 Hz), 8.26 (1H, s), 7.85 (2H, d, *J* = 8.6 Hz), 7.53−7.57 (4H, m), 7.48 (2H, d, *J* = 8.2 Hz), 7.34 (2H, t, *J* = 7.6 Hz), 4.44 (4H, q, *J* = 7.2 Hz), 1.51 (6H, t, *J* = 7.2 Hz). ^{13}C NMR (75 MHz, $CDCl_3$): δ 164.9, 162.1, 142.9, 141.7, 140.6, 132.1, 128.8, 127.9, 126.3, 125.1, 123.47, 123.29, 120.8, 119.71, 119.64, 119.34, 113.2, 109.7, 108.9, 108.6, 37.8, 14.0. UV−vis (CH_2Cl_2): λ_{max}^{abs} (ε) 365 (39 100), 349 (42 000), 302 (48 800), 279 nm (52 600). HR-ESI-TOF-MS: *m*/*z* calcd for $C_{39}H_{30}N_5^+$ 568.2501, found 568.2468 [(M + H)$^+$].

Preparation of 9-Ethyl-3-(2-{6-[2-(9-ethyl-9*H*-carbazol-3-yl)-ethynyl]pyrimidin-4-yl}ethynyl)-9*H*-carbazole (10). To a solution of **22** (0.36 g, 1.6 mmol) in Et_2O (5 mL) was added dropwise *n*-BuLi hexane solution (2.69 mol L^{-1}, 0.95 mL, 2.6 mmol) at −78 °C under argon atmosphere. After the mixture was stirred at −78 °C for 1 h, triisopropoxyborane (0.38 mL, 1.6 mmol) was added dropwise to the mixture at −78 °C. After the mixture was stirred at −78 °C for 2 h, a solution of 4,6-dichrolopyrimidine (81 mg, 0.54 mmol) and [$Pd(PPh_3)_4$] (40 mg, 35 μmol) in DME (10 mL) was added to the mixture. The resulting mixture was refluxed for 2.5 h. After addition of water (10 mL), the organic phase was separated, and the aqueous phase was extracted with toluene (10 mL × 3). The combined organic phase was washed with water (10 mL × 3), dried over anhydrous $MgSO_4$, and concentrated ender reduced pressure. The residue was purified by column chromatography (silica gel, toluene/EtOAc) to give **10** (0.19 g, 68%) as yellow solids. Mp 231−233 °C. ^{1}H NMR (400 MHz, $CDCl_3$): δ 9.17 (1H, d, *J* = 1.4 Hz), 8.41 (2H, d, *J* = 1.4 Hz), 8.11 (2H, d, *J* = 7.8 Hz), 7.73 (2H, dd, *J* = 8.5, 7.8 Hz), 7.64 (1H, d, *J* = 1.4 Hz), 7.52 (2H, ddd, *J* = 8.2, 7.1, 1.1 Hz), 7.42 (2H, d, *J* = 8.2 Hz), 7.39 (2H, d, *J* = 8.5 Hz), 7.30 (2H, ddd, *J* = 7.8, 7.1, 0.8 Hz), 4.35 (4H, q, *J* = 7.2 Hz), 1.45 (6H, t, *J* = 7.2 Hz). ^{13}C NMR (75 MHz, $CDCl_3$): δ 159.1, 151.2, 140.60, 140.45, 130.1, 126.5, 125.6, 124.9, 123.1, 122.4, 120.7, 119.8, 110.8, 108.96, 108.82, 97.3, 85.9, 37.8, 13.9. UV−vis (CH_2Cl_2): λ_{max}^{abs} (ε) 386 (55 800), 355 (40 400), 283 nm (53 500). HR-ESI-TOF-MS: *m*/*z* calcd for $C_{36}H_{27}N_4^+$ 515.2236, found 515.2188 [(M + H)$^+$].

Preparation of 9-Ethyl-3-(2-{6-[2-(9-ethyl-9*H*-carbazol-3-yl)-ethynyl]-2-(methylsulfanyl)pyrimidin-4-yl}ethynyl)-9*H*-carbazole (11). To a solution of **22** (0.53 g, 2.4 mmol) in Et_2O (15 mL) was added dropwise *n*-BuLi hexane solution (2.69 mol L^{-1}, 1.2 mL, 3.2 mmol) at −78 °C under argon atmosphere. After the mixture was stirred at −78 °C for 1 h, triisopropoxyborane (0.56 mL, 2.4 mmol) was added dropwise to the mixture at −78 °C. After the mixture was stirred at −78 °C for 1 h, a solution of 4,6-dichloro-2-(methylsulfanyl)pyrimidine (95 mg, 0.49 mmol) and [$Pd(PPh_3)_4$] (33 mg, 28 μmol) in DME (30 mL) was added to the mixture. The resulting mixture was refluxed for 17 h. After addition of water (10 mL), the organic phase was separated, and the aqueous phase was extracted with toluene (10 mL × 3). The combined organic phase was washed with water (10 mL × 3), dried over anhydrous $MgSO_4$, and concentrated ender reduced pressure. The residue was purified by column chromatography (silica gel, toluene) to give **11** (0.21 g, 76%) as yellow solids. Mp 210−211 °C. ^{1}H NMR (300 MHz, $CDCl_3$): δ 8.42 (2H, s), 8.12 (2H, d, *J* = 7.6 Hz), 7.74 (2H, d, *J* = 8.4 Hz), 7.53 (2H, t, *J* = 7.6 Hz), 7.44 (2H, d, *J* = 7.6 Hz), 7.41 (2H, d, *J* = 8.4 Hz), 7.34 (1H, s), 7.30 (2H, t, *J* = 7.6 Hz), 4.40 (4H, q, *J* = 7.2 Hz), 2.68 (3H, s), 1.47 (6H, t, *J* = 7.2 Hz). ^{13}C NMR (125 MHz, $CDCl_3$): δ 173.2, 151.2, 140.60, 140.49, 130.1, 126.5, 125.6, 123.1, 122.5, 120.8, 120.5, 119.9, 111.0, 108.99, 108.82, 96.9, 86.0, 37.8, 14.4, 13.9. UV−vis (CH_2Cl_2): λ_{max}^{abs} (ε) 396 (49 700), 355 (31 400), 307 nm (28 600), 284 (52 200). HR-ESI-TOF-MS: *m*/*z* calcd for $C_{37}H_{29}N_4S^+$561.2113, found 561.2096 [(M + H)$^+$].

Preparation of 9-Ethyl-3-(2-{6-[2-(9-ethyl-9*H*-carbazol-3-yl)-ethynyl]-2-methoxypyrimidin-4-yl}ethynyl)-9*H*-carbazole (12). To a suspension of NaH (60%, 27 mg, 0.67 mmol) in THF was added methanol (0.27 mL, 6.7 mmol) at 0 °C under argon atmosphere. Then, **14** (30 mg, 51 μmol) was added to the mixture. The resulting mixture was stirred at 0 °C for 1.5 h. After addition of water (10 mL), the organic phase was separated, and the aqueous phase was extracted with CH_2Cl_2 (10 mL × 3). The combined organic phase was washed with water (10 mL × 3), dried over anhydrous $MgSO_4$, and concentrated under reduced pressure. The residue was purified by column chromatography (silica gel, CH_2Cl_2) to give **12** (23 mg, 85%) as yellow solids. Mp 244−245 °C. ^{1}H NMR (400 MHz, $CDCl_3$): δ 8.41 (2H, d, *J* = 1.3 Hz), 8.12 (2H, d, *J* = 7.8 Hz), 7.74 (2H, dd, *J* = 8.5, 1.3 Hz), 7.52 (2H, ddd, *J* = 8.2, 7.1, 1.1 Hz), 7.45 (2H, d, *J* = 8.2 Hz), 7.42, (2H, d, *J* = 8.5 Hz), 7.34 (1H, s), 7.30 (2H, ddd, *J* = 7.8, 7.1, 1.0 Hz), 4.40 (4H, q, *J* = 7.2 Hz), 4.11 (3H, s), 1.47 (6H, t, *J* = 7.2 Hz). ^{13}C NMR (75 MHz, $CDCl_3$): δ 165.9, 153.2, 140.62, 140.52, 130.1, 126.5, 125.6, 123.2, 122.5, 120.8, 119.9, 119.4, 111.1, 108.99, 108.83, 96.5, 86.1, 55.3, 37.9, 14.0. UV−vis (CH_2Cl_2): λ_{max}^{abs} (ε) 390 (58 500), 355 (39 800), 281 nm (62 800). HR-ESI-TOF-MS: *m*/*z* calcd for $C_{37}H_{29}N_4O^+$ 545.2341, found 545.2321 [(M + H)$^+$].

Preparation of 9-Ethyl-3-(2-{6-[2-(9-ethyl-9*H*-carbazol-3-yl)-ethynyl]-2-(piperidin-1-yl)pyrimidin-4-yl}ethynyl)-9*H*-carbazole (13). A mixture of **14** (40 mg, 67 μmol) and piperidine (40 μL, 0.40 mmol) in 1,4-dioxane (5 mL) was stirred at room temperature for 4 h under argon atmosphere. After addition of water, the organic phase was separated, and the aqueous phase was extracted with toluene (10 mL × 3). The combined organic phase was washed with water (10 mL × 3), dried over anhydrous $MgSO_4$, and concentrated under reduced pressure. The residue was purified by column chromatography (silica gel, toluene) to give **13** (31 mg, 77%) as yellow solids. Mp 185−186 °C. ^{1}H NMR (300 MHz, $CDCl_3$): δ 8.40 (2H, d, *J* = 1.4 Hz), 8.11 (2H, d, *J* = 7.7 Hz), 7.72 (2H, dd, *J* = 8.5, 1.4 Hz), 7.51 (2H, ddd, *J* = 8.1, 7.2, 0.8 Hz), 7.43 (2H, d, *J* = 8.1 Hz), 7.40 (2H, d, *J* = 8.5 Hz), 7.31−7.26 (2H, m), 6.90 (1H, s), 4.38 (4H, q, *J* = 7.2 Hz), 3.92−3.90 (4H, m), 1.69 (6H, brs), 1.46 (6H, t, *J* = 7.2 Hz). ^{13}C NMR (75 MHz, $CDCl_3$): δ 161.8, 151.7, 140.47, 140.34, 130.0, 126.4, 125.3, 123.0, 122.6, 120.7, 119.7, 114.2, 111.7, 108.9, 108.6, 93.8, 86.8, 44.9, 37.8, 26.1, 25.0, 14.0. UV−vis (CH_2Cl_2): λ_{max} (ε) 397 (29 700), 353 (45 200), 305 (39 700). HR-ESI-TOF-MS: *m*/*z* calcd for $C_{41}H_{36}N_5^+$ 598.2971, found 598.2963 [(M + H)$^+$].

Preparation of 9-Ethyl-3-(2-{6-[2-(9-ethyl-9*H*-carbazol-3-yl)-ethynyl]-2-methanesulfonylpyrimidin-4-yl}ethynyl)-9*H*-carbazole (14). To a solution of **11** (30 mg, 54 μmol) in CH_2Cl_2 (10 mL)

DOI: 10.1021/acs.joc.5b01409
J. Org. Chem. 2015, 80, 9076−9090

was added *m*-chloroperoxybenzoic acid (66 mg, 0.29 mmol, 77%) at 0 °C. The resulting mixture was warmed to room temperature and stirred for 2.5 h. After addition of aqueous $Na_2S_2O_3$ (10%, 10 mL), the organic phase was separated, and the aqueous phase was extracted with CH_2Cl_2 (5 mL × 3). The combined organic phase was successively washed with aqueous $Na_2S_2O_3$ (10%, 5 mL × 3) and aqueous $NaHCO_3$ (1 mol L^{-1}, 5 mL × 3), dried over anhydrous $MgSO_4$, and concentrated under reduced pressure. The residue was purified by column chromatography (silica gel, CH_2Cl_2) to give **14** (32 mg, quant) as yellow solids. Mp 236−238 °C. ^{1}H NMR (400 MHz, $CDCl_3$): δ 8.42 (2H, d, J = 1.2 Hz), 8.12 (2H, d, J = 7.4 Hz), 7.75 (2H, dd, J = 8.0, 1.2 Hz), 7.70 (1H, s), 7.53 (2H, t, J = 7.2 Hz), 7.45 (2H, d, J = 7.4 Hz), 7.43 (2H, d, J = 8.0 Hz), 7.31 (2H, t, J = 8.0 Hz), 4.40 (4H, q, J = 7.2 Hz), 3.45 (3H, s), 1.47 (6H, t, J = 7.2 Hz). ^{13}C NMR (75 MHz, $CDCl_3$): δ 166.2, 152.4, 140.9, 140.5, 130.3, 126.86, 126.75, 125.9, 123.2, 122.4, 120.8, 120.1, 110.2, 109.0, 108.9, 101.0, 85.7, 39.4, 37.9, 13.9. UV−vis (CH_2Cl_2): λ_{max}^{abs} (ε) 417 (50 800), 355 (17 100), 321 (24 400), 293 (42 500), 273 nm (40 400). HR-ESI-TOF-MS: m/z calcd for $C_{37}H_{29}N_4O_2S^+$ 593.2011, found 593.1987 [(M + H)$^+$].

Preparation of 4,6-Bis[2-(9-ethyl-9*H*-carbazol-3-yl)ethynyl]-pyrimidine-2-carbonitrile (15). A mixture of **14** (30 mg, 51 μmol) and KCN (4 mg, 61 μmol) in DMF (10 mL) was stirred at −5 °C for 2 h under argon atmosphere. After addition of saturated aqueous $NaHCO_3$ (10 mL), the organic phase was separated, and the aqueous phase was extracted with CH_2Cl_2 (10 mL × 3). The combined organic phase was washed with saturated aqueous $NaHCO_3$ (50 mL × 3), dried over anhydrous Na_2SO_4, and concentrated under reduced pressure. The residue was purified by column chromatography (silica gel, toluene) to give **15** (15 mg, 55%) as yellow solids. Mp 275 °C (decomp). ^{1}H NMR (400 MHz, $CDCl_3$): δ 8.44 (2H, d, J = 1.4 Hz), 8.12 (2H, d, J = 7.6 Hz), 7.75 (2H, dd, J = 8.5, 1.4 Hz), 7.73 (1H, s), 7.54 (2H, t, J = 7.7 Hz), 7.46 (2H, d, J = 7.7 Hz) 7.45 (2H, d, J = 8.5 Hz), 7.31 (2H, d, J = 7.7 Hz) 4.41 (4H, q, J = 7.2 Hz), 1.48 (6H, t, J = 7.2 Hz). ^{13}C NMR (75 MHz, $CDCl_3$): δ 152.3, 141.0, 140.5, 130.3, 126.8, 126.6, 126.1, 123.3, 122.4, 120.8, 120.1, 110.1, 109.12, 109.03, 100.7, 85.2, 38.0, 14.0 (18 signals out of 20 expected). UV−vis (CH_2Cl_2): λ_{max}^{abs} (ε) 415 (54 100), 355 (19 100), 322 (24 900), 293 (39 800), 274 nm (26 300). HR-ESI-TOF-MS: m/z calcd for $C_{37}H_{26}N_5^+$ 540.2188, found 540.2202 [(M + H)$^+$].

Preparation of 9-Ethyl-3-[(*E*)-2-{6-[(*E*)-2-(9-ethyl-9*H*-carbazol-3-yl)ethenyl]pyrimidin-4-yl}ethenyl]-9*H*-carbazole (16). To a solution of **22** (0.34 g, 1.5 mmol) in THF (20 mL) was added catecholborane THF solution (1 mol L^{-1}, 3.2 mL, 3.2 mmol) at room temperature under argon atmosphere. The mixture was refluxed for 8 h under the light protection. After 4,6-dichlolopyrimidine (0.75 g, 0.50 mmol), aqueous $NaHCO_3$ (2 mol L^{-1}, 3 mL) and [$Pd(PPh_3)_4$] (35 mg, 30 μmol) were successively added to the mixture at room temperature, and the resulting mixture was refluxed for 12 h under the light protection. After addition of water (20 mL), the aqueous phase was extracted with toluene (50 mL × 3). The organic phase was washed with water (30 mL × 2), dried over anhydrous Na_2SO_4, and concentrated under reduced pressure. The residue was purified by repeated column chromatography (silica gel, toluene) to give **16** (44 mg, 16%) as yellow solids. Mp 242−243 °C. ^{1}H NMR (300 MHz, $CDCl_3$): δ 9.11 (1H, s), 8.34 (2H, d, J = 1.5 Hz), 8.15 (2H, d, J = 6.7 Hz), 8.11 (2H, d, J = 15.6 Hz), 7.77 (2H, dd, J = 8.6, 1.5 Hz), 7.51 (2H, ddd, J = 8.1, 7.0, 1.1 Hz), 7.42 (2H, d, J = 8.1 Hz), 7.41 (2H, d, J = 8.6 Hz), 7.31−7.26 (3H, m), 7.11 (2H, d, J = 15.6 Hz), 4.37 (4H, q, J = 7.2 Hz), 1.46 (6H, t, J = 7.2 Hz); ^{13}C NMR (75 MHz, $CDCl_3$): δ 163.1, 158.7, 140.8, 140.5, 138.0, 127.0, 126.2, 125.6, 123.5, 123.12, 123.03, 120.68, 120.49, 119.5, 115.8, 108.96, 108.93, 37.8, 14.0. UV−vis (CH_2Cl_2): λ_{max}^{abs} (ε) 405 (55 200), 294 nm (49 600). HR-ESI-TOF-MS: m/z calcd for $C_{36}H_{31}N_4^+$ 519.2549, found 519.2557 [(M + H)$^+$].

Preparation of 9-Ethyl-3-[(*E*)-2-{6-[(*E*)-2-(9-ethyl-9*H*-carbazol-3-yl)ethenyl]-2-(methylsulfanyl)pyrimidin-4-yl}ethenyl]-9*H*-carbazole (17). To a solution of **22** (0.71 g, 3.3 mmol) in THF (30 mL) was added catecholborane THF solution (1 mol L^{-1}, 7.0 mL, 7.0 mmol) at room temperature under argon atmosphere. The mixture was refluxed for 8 h under the light protection. After 4,6-dichloro-2-(methylsulfanyl)pyrimidine (0.21 g, 1.1 mmol), aqueous $NaHCO_3$ (2 mol L^{-1}, 5 mL), and [$Pd(PPh_3)_4$] (75 mg, 65 μmol) were successively added to the mixture at room temperature, the resulting mixture was refluxed for 11 h under the light protection. After addition of water (20 mL), the aqueous phase was extracted with toluene (50 mL × 3). The organic phase was washed with water (30 mL × 2), dried over anhydrous Na_2SO_4, and concentrated under reduced pressure. The residue was purified by column chromatography (silica gel, toluene) and washed with toluene (2 mL × 5) to give **17** (0.46 g, 76%) as yellow solids. Mp 209−210 °C. ^{1}H NMR (300 MHz, $CDCl_3$): δ 8.34 (2H, d, J = 1.4 Hz), 8.14 (2H, d, J = 7.4 Hz), 8.11 (2H, d, J = 15.7 Hz), 7.77 (2H, dd, J = 8.5, 1.4 Hz), 7.51 (2H, ddd, J = 8.1, 7.1, 1.0 Hz), 7.43 (2H, d, J = 8.1 Hz), 7.42 (2H, d, J = 8.5 Hz), 7.31−7.26 (2H, m), 7.07 (2H, d, J = 15.7 Hz), 7.01 (2H, s), 4.38 (4H, q, J = 7.2 Hz), 2.75 (3H, s), 1.47 (6H, t, J = 7.2 Hz). ^{13}C NMR (75 MHz, $CDCl_3$): δ 163.2, 140.79, 140.55, 138.1, 127.1, 126.2, 125.6, 123.5, 123.20, 123.08, 120.70, 120.59, 119.5, 111.4, 108.9, 37.8, 14.4, 14.0 (18 signals out of 20 expected). UV−vis (CH_2Cl_2): λ_{max}^{abs} (ε) 409 (53 200), 294 nm (52 700). HR-ESI-TOF-MS: m/z calcd for $C_{37}H_{33}N_4S^+$ 565.2426, found 565.2440 [(M + H)$^+$].

■ ASSOCIATED CONTENT

Supporting Information

. The Supporting Information is available free of charge on the ACS Publications website at DOI: 10.1021/acs.joc.5b01409.

General experimental methods, complete photophysical and electrochemical data, theoretical data, ^{1}H and ^{13}C NMR data of all new compounds, and recycling GPC profiles (PDF)

3D structures of **1**−**17** (XYZ)

Crystallographic information of **3** (CIF)

Crystallographic information of **6** (CIF)

Crystallographic information of **11** (CIF)

Crystallographic information of **14** (CIF)

■ AUTHOR INFORMATION

Corresponding Author

*E-mail: nakamura@gunma-u.ac.jp. Phone: +81 277 30 1310. Fax: +81 277 30 1314.

Notes

The authors declare no competing financial interest.

■ ACKNOWLEDGMENTS

This work was supported by a Grant-in-Aid for Scientific Research from the Ministry of Education, Culture, Sports, Science and Technology of Japan (No. 24550040, 15K05416), and partially performed under the Cooperative Research Program of "Network Joint Research Center for Materials and Devices" (Kyushu University: No. 2015474). Quantum chemical calculations were performed in the Research Center for Computational Science, Japan. The authors thank Prof. Seiji Tobita (Gunma University) for generous permission to use an integrating sphere system for the determination of absolute fluorescence quantum yields of the compounds in the present work.

■ REFERENCES

(1) (a) *Organic Electronics: Materials, Manufacturing and Applications*; Klauk, H., Eds.; Wiley-VCH: Weinheim, 2006. (b) *Organic Light Emitting Devices: Synthesis, Properties and Applications*; Müllen, K., Scherf, U., Eds.; Wiley-VCH: Weinheim, 2006. (c) *Functional Organic Materials*; Müller, T. J. J., Bunz, U. H. F., Eds.; Wiley-VCH: Weinheim, 2007. (d) *Organic Electroluminescence*; Kakafi, Z. H., Eds.; CRC Press: New York, 2005. (e) *Carbon-Rich Compounds: From Molecules to*

DOI: 10.1021/acs.joc.5b01409
J. Org. Chem. 2015, 80, 9076−9090

Materials; Haley, M. M., Tykwinski, R. R., Eds.; Wiley-VCH: Weinheim, 2006.
(2) (a) Kelley, T. W.; Baude, P. F.; Gerlach, C.; Ender, D. E.; Muyres, D.; Haase, M. A.; Vogel, D. E.; Theiss, S. D. *Chem. Mater.* **2004**, *16*, 4413. (b) Special issue on Organic Electronics and Optoelectronics; Forrest, S. R., Thompson, M. E., Eds.: *Chem. Rev.* **2007**, *107*, 923, DOI: 10.1021/cr0501590. (c) Bendikov, M.; Wudl, F.; Perepichka, D. F. *Chem. Rev.* **2004**, *104*, 4891. (d) Shirota, Y.; Kageyama, H. *Chem. Rev.* **2007**, *107*, 953. (e) Wu, W.; Liu, Y.; Zhu, D. *Chem. Soc. Rev.* **2010**, *39*, 1489.
(3) For reviews, see: (a) Meier, H. *Angew. Chem., Int. Ed.* **2005**, *44*, 2482. (b) Grimsdale, A. C.; Chan, K. L.; Martin, R. E.; Jokisz, P. G.; Holmes, A. B. *Chem. Rev.* **2009**, *109*, 897. (c) Arias, A. C.; MacKenzie, J. D.; McCulloch, I.; Rivnay, J.; Salleo, A. *Chem. Rev.* **2010**, *110*, 3. (d) Li, C.; Liu, M.; Pschirer, N. G.; Baumgarten, M.; Müllen, K. *Chem. Rev.* **2010**, *110*, 6817.
(4) For reviews, see: (a) Grazulevicius, J. V.; Strohriegl, P.; Pielichowski, J.; Pielichowski, K. *Prog. Polym. Sci.* **2003**, *28*, 1297. (b) Morin, J.-F.; Leclerc, M.; Adès, D.; Siove, A. *Macromol. Rapid Commun.* **2005**, *26*, 761. (c) Blouin, N.; Leclerc, M. *Acc. Chem. Res.* **2008**, *41*, 1110. (d) Boudreault, P.-L. T.; Morin, J.-F.; Leclerc, M. In *Design and Synthesis of Conjugated Polymers*; Leclerc, M., Morin, J.-F., Eds.; Wiley-VCH: Weinheim, 2010; p 205.
(5) Inter alia: (a) Kulkarni, A. P.; Kong, X.; Jenekhe, S. A. *Adv. Funct. Mater.* **2006**, *16*, 1057. (b) Lin, S.-L.; Chan, L.-H.; Lee, R.-H.; Yen, M.-Y.; Kuo, W.-J.; Chen, C.-T.; Jeng, R.-J. *Adv. Mater.* **2008**, *20*, 3947. (c) Palayangoda, S. S.; Cai, X.; Adhikari, R. M.; Neckers, D. C. *Org. Lett.* **2008**, *10*, 281. (d) Adhikari, R. M.; Neckers, D. C.; Shah, B. K. *J. Org. Chem.* **2009**, *74*, 3341. (e) Moss, K. C.; Bourdakos, K. N.; Bhalla, V.; Kamtekar, K. T.; Bryce, M. R.; Fox, M. A.; Vaughan, H. L.; Dias, F. B.; Monkman, A. P. *J. Org. Chem.* **2010**, *75*, 6771. (f) Panthi, K.; Adhikari, R. M.; Kinstle, T. H. *J. Phys. Chem. A* **2010**, *114*, 4542. (g) Prachumrak, N.; Pojanasopa, S.; Namuangruk, S.; Kaewin, T.; Jungsuttiwong, S.; Sudyoadsuk, T.; Promarak, V. *ACS Appl. Mater. Interfaces* **2013**, *5*, 8694.
(6) Uoyama, H.; Goushi, K.; Shizu, K.; Nomura, H.; Adachi, C. *Nature* **2012**, *492*, 234.
(7) For a review, see: Tao, Y.; Yuan, K.; Chen, T.; Xu, P.; Li, H.; Chen, R.; Zheng, C.; Zhang, L.; Huang, W. *Adv. Mater.* **2014**, *26*, 7931 and references cited therein.
(8) Inter alia: (a) Zhang, Q.; Li, J.; Shizu, K.; Huang, S.; Hirata, S.; Miyazaki, H.; Adachi, C. *J. Am. Chem. Soc.* **2012**, *134*, 14706. (b) Nishimoto, T.; Yasuda, T.; Lee, S. Y.; Kondo, R.; Adachi, C. *Mater. Horiz.* **2014**, *1*, 264. (c) Shizu, K.; Tanaka, H.; Uejima, M.; Sato, T.; Tanaka, K.; Kaji, H.; Adachi, C. *J. Phys. Chem. C* **2015**, *119*, 1291. (d) Suzuki, Y.; Zhang, Q.; Adachi, C. *J. Mater. Chem. C* **2015**, *3*, 1700. (e) Albrecht, K.; Matsuoka, K.; Fujita, K.; Yamamoto, K. *Angew. Chem., Int. Ed.* **2015**, *54*, 5677.
(9) For a review, see: Achelle, S.; Plé, N. *Curr. Org. Synth.* **2012**, *9*, 163.
(10) (a) Wong, K.-T.; Hsu, C. C. *Org. Lett.* **2001**, *3*, 173. (b) Wong, K.-T.; Hung, T. S.; Lin, Y.; Wu, C.-C.; Lee, G.-H.; Peng, S.-M.; Chou, C. H.; Su, Y. O. *Org. Lett.* **2002**, *4*, 513. (c) Itami, K.; Yamazaki, D.; Yoshida, J. *J. Am. Chem. Soc.* **2004**, *126*, 15396. (d) Pascal, L.; Vanden Eynde, J. J.; Van Haverbeke, Y. V.; Dubois, P.; Michel, A.; Rant, U.; Zojer, E.; Leising, G.; Van Dorn, L. O.; Gruhn, N. E.; Cornil, J.; Brédas, J.-L. *J. Phys. Chem. B* **2002**, *106*, 6442.
(11) (a) Dufresne, S.; Hanan, G. S.; Skene, W. G. *J. Phys. Chem. B* **2007**, *111*, 11407. (b) Achelle, S.; Ramondenc, Y.; Marsais, F.; Plé, N. *Eur. J. Org. Chem.* **2008**, *2008*, 3129. (c) Bagley, M. C.; Lin, Z.; Pope, S. J. A. *Tetrahedron Lett.* **2009**, *50*, 6818. (d) Achelle, S.; Kahlal, S.; Saillard, J.-Y.; Cabon, N.; Caro, B.; Robin-le Guen, F. *Tetrahedron* **2014**, *70*, 2804.
(12) (a) Liu, Z.; Chen, T.; Liu, B.; Huang, Z.-L.; Huang, T.; Li, S.; Xu, Y.; Qin, J. *J. Mater. Chem.* **2007**, *17*, 4685. (b) Li, L.; Tian, Y.-P.; Yang, J.-X.; Sun, P.-P.; Wu, J.-Y.; Zhou, H.-P.; Zhang, S.-Y.; Jin, B.-K.; Xing, X.-J.; Wang, C.-K.; Li, M.; Cheng, G.-H.; Tang, H.-H.; Huang, W.-H.; Tao, X.-T.; Jiang, M.-H. *Chem. - Asian J.* **2009**, *4*, 668. (c) Achelle, S.; Nouira, I.; Pfaffinger, B.; Ramondenc, Y.; Plé, N.; Rodríguez-López, J. *J. Org. Chem.* **2009**, *74*, 3711. (d) Hadad, C.; Achelle, S.; García-Martinez, J. C.; Rodríguez-López, J. *J. Org. Chem.* **2011**, *76*, 3837. (e) Achelle, S.; Barsella, A.; Baudequin, C.; Caro, B.; Robin-le Guen, F. *J. Org. Chem.* **2012**, *77*, 4087. (f) Chen, D.; Zhong, C.; Dong, X.; Liu, Z.; Qin, J. *J. Mater. Chem.* **2012**, *22*, 4343. (g) Li, L.; Ge, J.; Wu, H.; Xu, Q.-H.; Yao, S. Q. *J. Am. Chem. Soc.* **2012**, *134*, 12157. (h) Tang, C.; Zhang, Q.; Li, D.; Zhang, J.; Shi, P.; Li, S.; Wu, J.; Tian, Y. *Dyes Pigm.* **2013**, *99*, 20. (i) Achelle, S.; Malval, J.-P.; Aloïse, S.; Barsella, A.; Spangenberg, A.; Mager, L.; Akdas-Kilig, H.; Fillaut, J.-L.; Caro, B.; Robin-le Guen, F. *ChemPhysChem* **2013**, *14*, 2725. (j) Wang, A.; Long, L.; Meng, S.; Li, X.; Zhao, W.; Song, Y.; Cifuentes, M. P.; Humphrey, M. G.; Zhang, C. *Org. Biomol. Chem.* **2013**, *11*, 4250. (k) Malval, J.-P.; Achelle, S.; Bodiou, L.; Spangenberg, A.; Gomez, L. C.; Soppera, O.; Robin-le Guen, F. *J. Mater. Chem. C* **2014**, *2*, 7869.
(13) (a) Achelle, S.; Ramondenc, Y.; Dupas, G.; Plé, N. *Tetrahedron* **2008**, *64*, 2783. (b) Achelle, S.; Plé, N.; Kreher, D.; Attias, A.-J.; Arfaoui, I.; Charra, F. *Tetrahedron Lett.* **2009**, *50*, 7055. (c) Malik, I.; Ahmed, Z.; Reimann, S.; Ali, I.; Villinger, A.; Langer, P. *Eur. J. Org. Chem.* **2011**, *2011*, 2088. (d) Martin, F.-A.; Baudequin, C.; Fiol-Petit, C.; Darabantu, M.; Ramondenc, Y.; Plé, N. *Tetrahedron* **2014**, *70*, 2546.
(14) Weng, J.; Mei, Q.; Zhang, B.; Jiang, Y.; Tong, B.; Fan, Q.; Ling, Q.; Huang, W. *Analyst* **2013**, *138*, 6607.
(15) (a) Aizawa, N.; Pu, Y.-J.; Sasabe, H.; Kido, J. *Org. Electron.* **2012**, *13*, 2235. (b) Su, S.-J.; Cai, C.; Kido, J. *J. Mater. Chem.* **2012**, *22*, 3447. (c) Weng, J.; Mei, Q.; Fan, Q.; Ling, Q.; Tong, B.; Huang, W. *RSC Adv.* **2013**, *3*, 21877. (d) Verbitskiy, E. V.; Cheprakova, E. M.; Subbotina, J. O.; Schepochkin, A. V.; Slepukhin, P. A.; Rusinov, G. L.; Charushin, V. N.; Chupakhin, O. N.; Makarova, N. I.; Metelitsa, A. V.; Minkin, V. I. *Dyes Pigm.* **2014**, *100*, 201. (e) Hao, Q.; Yu, S.; Li, S.; Chen, J.; Zeng, Y.; Yu, T.; Yang, G.; Li, Y. *J. Org. Chem.* **2014**, *79*, 459. (f) Skardziute, L.; Dodonova, J.; Voitechovicius, A.; Jovaisaite, J.; Komskis, R.; Voitechoviciute, A.; Bucevicius, J.; Kazlauskas, K.; Jursenas, S.; Tumkevicius, S. *Dyes Pigm.* **2015**, *118*, 118. (g) Syutkin, R. V.; Abashev, G. G.; Shklyaeva, E. V.; Kudryavtsev, P. G. *Russ. J. Org. Chem.* **2011**, *47*, 530.
(16) (a) Shimizu, H.; Kobayashi, A.; Itoi, S.; Yoshihara, T.; Tobita, S.; Nakamura, Y.; Nishimura, J. *Heterocycles* **2009**, *78*, 1265. (b) Shimizu, Y.; Kakinoya, Y.; Takehira, T.; Yoshihara, T.; Tobita, S.; Nakamura, Y.; Nishimura, J. *Bull. Chem. Soc. Jpn.* **2009**, *82*, 860. (c) Kato, S.-i.; Shimizu, S.; Taguchi, H.; Kobayashi, A.; Tobita, S.; Nakamura, Y. J. *J. Org. Chem.* **2012**, *77*, 3222. (d) Kato, S.-i.; Noguchi, H.; Kobayashi, A.; Yoshihara, T.; Tobita, S.; Nakamura, Y. J. *J. Org. Chem.* **2012**, *77*, 9120. (e) Kato, S.-i.; Shimizu, S.; Kobayashi, A.; Yoshihara, T.; Tobita, S.; Nakamura, Y. J. *J. Org. Chem.* **2014**, *79*, 618.
(17) Saygili, N.; Batsanov, A. S.; Bryce, M. R. *Org. Biomol. Chem.* **2004**, *2*, 852.
(18) Van Rossom, W.; Maes, W.; Kishore, L.; Ovaere, M.; Van Meervelt, L.; Dehaen, W. *Org. Lett.* **2008**, *10*, 585.
(19) Liebeskind, L. S.; Srogl, J. *Org. Lett.* **2002**, *4*, 979.
(20) We observed no reaction of phenylboronic acid pinacol ester with **2**.
(21) Castanet, A.-S.; Colobert, F.; Schlama, T. *Org. Lett.* **2000**, *2*, 3559.
(22) Stoll, R. S.; Peters, M. V.; Kuhn, A.; Heiles, S.; Goddard, R.; Bühl, M.; Thiele, C. M.; Hecht, S. J. *J. Am. Chem. Soc.* **2009**, *131*, 357.
(23) The yields of **16** and **17** as stereoisomer mixtures after the silica gel column chromatography are 81% and 98%, respectively. Compounds **16** and **17** with *E,Z*- and/or *Z,Z*- configuration were found to exist in ca. 10% in the mixtures on the basis of the ^{1}H NMR spectral measurements.
(24) The photostability of *E,E*-**16** is discussed in the Supporting Information.
(25) For detail about the conformation of carbazole−pyrimidine conjugates, see the Supporting Information (Figures S21−S23).
(26) Multiple CH−π interactions are also observable.
(27) For the insulating effects of acetylenic segments, see: (a) Moonen, N. N. P.; Diederich, F. *Org. Biomol. Chem.* **2004**, *2*,

DOI: 10.1021/acs.joc.5b01409
J. Org. Chem. 2015, 80, 9076−9090

2263. (b) Moonen, N. N. P.; Pomerantz, W. C.; Gist, R.; Boudon, C.; Gisselbrecht, J.-P.; Seiler, P.; Kawai, T.; Kishioka, A.; Gross, M.; Irie, M.; Diederich, F. *Chem. - Eur. J.* **2005**, *11*, 3325.

(28) For the effects of the ethynylene and vinylene units on the HOMO−LUMO gap in the push−pull systems, see: Frank, B. B.; Laporta, P. R.; Breiten, B.; Kuzyk, M. C.; Jarowski, P. D.; Schweizer, W. B.; Seiler, P.; Biaggio, I.; Boudon, C.; Gisselbrecht, J.-P.; Diederich, F. *Eur. J. Org. Chem.* **2011**, *2011*, 4307.

(29) The $E_T(30)$ parameters (33.9 kcal mol^{-1} for toluene, 37.4 kcal mol^{-1} for THF, 38.1 kcal mol^{-1} for EtOAc, 40.7 kcal mol^{-1} for CH_2Cl_2, 42.9 kcal mol^{-1} for DMF) are taken from: Reichardt, C. *Chem. Rev.* **1994**, *94*, 2319.

(30) Reichardt, C.; Welton, T. *Solvents and Solvent Effects in Organic Chemistry*, 4th ed.; Wiley-VCH: Weinheim, 2011.

(31) We confirmed that Reichardt plots compared to Lippert−Mataga plots gave high goodness of fit parameters r^2.

(32) It is unclear at present whether **1** in CH_2Cl_2 is mono- or diprotonated upon addition of excess amount of TFA.[12c−e]

(33) The protonated species are apparently more polar than the neutral ones, and the photophysical properties of the former should be more sensitive to the solvent polarity than the latter. Thus, the observed gradual red-shifts of new absorption and fluorescence bands with increasing TFA may be explained by solvatochromism. See also ref 12c.

(34) The HOMO and LUMO levels of monoprotonated **1** are calculated to be −8.16 eV and −5.48 eV, respectively, at the B3LYP/6-311G(d,p)//B3LYP/6-31G(d) level. The decrease in the LUMO level is larger than that in the HOMO level from the neutral **1** to the monoprotonated **1**.

(35) It is considered that the protonation of the piperidyl nitrogen atom also occurs in **4**: Zucchero, A. J.; McGrier, P. L.; Bunz, U. H. F. *Acc. Chem. Res.* **2010**, *43*, 397.

(36) Mazik, M.; Zielinski, W. *Monatsh. Chem.* **1996**, *127*, 587.

(37) The decreased electronic communication between the carbazole (donor) and pyrimidine (acceptor) moieties caused by the insertion of the spacers is considered to be responsible for both the positive shifts of the E_{red} values of **10**−**15**, **16**, and **17** relative to those of the corresponding **1**−**6** and the negative shifts of the E_{ox} values of **16** and **17** relative to those of **1** and **2**, respectively. The reason for the positive shifts of the E_{ox} values of **10**−**15** as compared to the corresponding **1**−**6** may be that the electron-withdrawing effect of an ethynylene unit exceeds its effect to weaken the D−A communication.

(38) All calculations were carried out using Gaussian 09, Revision B.01: Frisch, M. J.; Trucks, G. W.; Schlegel, H. B.; Scuseria, G. E.; Robb, M. A.; Cheeseman, J. R.; Scalmani, G.; Barone, V.; Mennucci, B.; Petersson, G. A.; Nakatsuji, H.; Caricato, M.; Li, X.; Hratchian, H. P.; Izmaylov, A. F.; Bloino, J.; Zheng, G.; Sonnenberg, J. L.; Hada, M.; Ehara, M.; Toyota, K.; Fukuda, R.; Hasegawa, J.; Ishida, M.; Nakajima, T.; Honda, Y.; Kitao, O.; Nakai, H.; Vreven, T.; Montgomery, J. A., Jr.; Peralta, J. E.; Ogliaro, F.; Bearpark, M.; Heyd, J. J.; Brothers, E.; Kudin, K. N.; Staroverov, V. N.; Keith, T.; Kobayashi, R.; Normand, J.; Raghavachari, K.; Rendell, A.; Burant, J. C.; Iyengar, S. S.; Tomasi, J.; Cossi, M.; Rega, N.; Millam, J. M.; Klene, M.; Knox, J. E.; Cross, J. B.; Bakken, V.; Adamo, C.; Jaramillo, J.; Gomperts, R.; Stratmann, R. E.; Yazyev, O.; Austin, A. J.; Cammi, R.; Pomelli, C.; Ochterski, J. W.; Martin, R. L.; Morokuma, K.; Zakrzewski, V. G.; Voth, G. A.; Salvador, P.; Dannenberg, J. J.; Dapprich, S.; Daniels, A. D.; Farkas, O.; Foresman, J. B.; Ortiz, J. V.; Cioslowski, J.; Fox, D. J. *Gaussian 09, Revision B.01*; Gaussian, Inc., Wallingford CT, 2010.

(39) The deviation from planarity of **13** in the crystalline state, where the dihedral angle of ca. 10° between the pyrimidine and carbazole moieties is present, is attributable to the crystal packing force.

(40) Considering SMe, OMe, and phenyl groups as inductive substituents, they can be recognized as electron-withdrawing groups. For inductive substituent constants, see: Grob, C. A; Schaub, B.; Schlageter, M. G. *Helv. Chim. Acta* **1980**, *63*, 57.

(41) The oscillator strength (f) for the HOMO−LUMO transition of **9** is calculated to be 0.0003, which is substantially smaller than the f values of **1**−**8** and **10**−**17** to be 0.39−1.31. The f value for the HOMO−LUMO + 1 transition of **9** is estimated to be 0.55.

(42) It is likely that the ΔE_{opt} value of **9** is the energy corresponding to the HOMO−LUMO + 1 transition, whereas its ΔE_{redox} value is the energy difference between the HOMO and the LUMO levels. This should bring about the large deviation of **9** from the linear correlation in Figure S20a in the Supporting Information.

DOI: 10.1021/acs.joc.5b01409
J. Org. Chem. 2015, 80, 9076−9090